Theory of stoichiometric intraguild predation: algae, ciliate, and *Daphnia*

Shufei Gao[1], Hao Wang[2], Sanling Yuan[1*]

[1]College of Science, University of Shanghai for Science and Technology, Shanghai 200093, China.
[2]Department of Mathematical and Statistical Sciences, University of Alberta, Edmonton, Alberta T6G 2G1, Canada.

*Corresponding author(s). E-mail(s): sanling@usst.edu.cn;

Abstract

Consumers respond differently to external nutrient changes than producers, resulting in a mismatch in elemental composition between them and potentially having a significant impact on their interactions. To explore the responses of herbivores and omnivores to changes in elemental composition in producers, we develop a novel stoichiometric model with an intraguild predation structure. The model is validated using experimental data, and the results show that our model can well capture the growth dynamics of these three species. Theoretical and numerical analyses reveal that the model exhibits complex dynamics, including chaotic-like oscillations and multiple types of bifurcations, and undergoes long transients and regime shifts. Under moderate light intensity and phosphate concentration, these three species can coexist. However, when the light intensity is high or the phosphate concentration is low, the energy enrichment paradox occurs, leading to the extinction of ciliate and *Daphnia*. Furthermore, if phosphate is sufficient, the competitive effect of ciliate and *Daphnia* on algae will be dominant, leading to competitive exclusion. Notably, when the phosphorus-to-carbon ratio of ciliate is in a suitable range, the energy enrichment paradox can be avoided, thus promoting the coexistence of species. These findings contribute to a deeper understanding of species coexistence and biodiversity.

Keywords: Ecological stoichiometry, Intraguild predation model, Food quality, Phosphorus, Light

MSC Classification: 92B05 , 92D25 , 92D40

1 Introduction

Alterations in nutrient supply, driven by eutrophication and climate warming, can modify the elemental composition of primary producers and have effects on higher trophic levels through energy and material transfer in the food web (De Senerpont Domis et al, 2014; Tong et al, 2020). In general, the elemental composition of primary producers is flexible and very sensitive to changes in the nutritional status of the external environment (Paul et al, 2016). In contrast, most consumers can regulate and maintain their elemental ratios and have more stable cell quotas than primary producers (Sterner and Elser, 2017). This stoichiometric mismatch may bear significant consequences for interactions between consumers and their food resources, further impacting material and energy cycling in ecosystems (Sterner and Elser, 2017). For instance, some studies illustrated that poor-quality producers, characterized by a lower phosphorus-to-carbon ratio, may lead to the extinction of consumers (Diehl et al, 2022; Liu et al, 2023). Therefore, it is necessary and interesting to explore the effects of changes in element ratios in producers on predators or higher trophic levels, which can deepen our understanding of the coexistence mechanism of species and ecosystem stability.

Ecological stoichiometry serves as a powerful tool for describing the balance of nutrients (phosphorus and nitrogen) and energy (light and carbon) in ecosystems and can help us understand the impact of environmental changes on food webs (Sterner and Elser, 2017). In the field of mathematical modeling, the stoichiometry model has garnered widespread interest, with a growing number of researchers integrating stoichiometry into ecological models to elucidate various ecological phenomena and existing paradoxes (Peace et al, 2013; Yan et al, 2022; Loladze et al, 2000; Chen et al, 2017). One notable example is the Lotka-Volterra type producer-grazer stoichiometry model, originally proposed by Loladze et al (2000), which tracks the quantity and quality of producers. This model revealed the presence of energy enrichment paradox, i.e., eating large amounts of low-quality food can lead to the extinction of predators. Then, Li et al (2011) and Xie et al (2018) conducted a comprehensive global analysis and bifurcation analysis of the LKE model by considering Holling type I and Holling type II functional response functions, respectively. Building upon the work of Xie et al (2018), Yuan et al (2020) further explored the impact of environmental noise by developing a stochastically producer-grazer model. They investigated the phenomenon of regime shift between two stochastic attractors induced by noise in a bistable region. Furthermore, Peace et al (2014) extended the LKE model to study the growth response of *Daphnia* to algae with varying quality by tracking phosphate (P_i) levels in producers and the environment.

Most of the aforementioned models introduce stoichiometry into predation and competition models to study these two basic community relationships. Besides predation and competition, another basic community relationship, known as intraguild predation (IGP), has garnered substantial attention from both theoretical and empirical ecologists (Polis and Holt, 1992; Arim and Marquet, 2004; Hall, 2011; Lonsinger et al, 2017; Pringle et al, 2019; Diehl et al, 2022). It is a mixture of competition and predation, i.e., two species that compete for shared resources, and also involves a predator-prey relationship (Holt and Polis, 1997). Usually, three species are included

in the community relationship of IGP: intraguild (IG) predator, IG prey, and their shared prey species. There are numerous examples of IGP in both aquatic and terrestrial food web ecosystems. For instance, in aquatic ecosystems, ciliate and *Daphnia* both consume algae, but *Daphnia* also preys on ciliate (Diehl et al, 2022). Based on this community relationship, a large number of mathematical models have been developed. Holt and Polis (1997), to study the mechanism of species coexistence, first constructed a three-species food web model with IGP structure, revealing the challenges faced in achieving stable three-species coexistence. Subsequently, a large number of researchers conducted modeling and dynamics analysis of IGP from different perspectives (Ji et al, 2022; Hsu et al, 2015; Shu et al, 2015; Kang and Wedekin, 2013; Diehl, 2003). In addition, to consider the impact of nutrients on food webs with IGP structures, some researchers have introduced stoichiometry into the IGP models. For instance, Diehl (2003) established a model consisting of one plant species with a flexible nutrient stoichiometry and two herbivorous consumers with fixed stoichiometry, delving into the mechanism for the coexistence of these three species. Ji et al (2023) formulated a stoichiometric IGP model that incorporates environmental fluctuations. Their results showed that the model can exhibit intricate dynamics, encompassing various forms of bifurcation and numerous types of bistability, especially cycle-cycle bistability, which does not appear in the non-stoichiometric IGP model. Taking into account changes in time scales, Chen et al (2023) constructed a discrete-time stoichiometric IGP model. Their investigation illuminated the differences in multistability characteristics and the existence interval of chaos between discrete-time and continuous-time models under moderate and high light intensities.

These stoichiometric IGP models assume that all phosphate (P_i) in the system is within the bodies of the three species while ignoring free P_i in the environment. This assumption gives rise to a problem for the stoichiometric IGP model. Assuming that all available P_i is in the producer, then if its biomass is low, the P_i cell quota Q of the producer will become unrealistically large. To tackle this issue, a feasible way is to introduce the maximum value of Q. Consequently, two supplementary equations must be incorporated to trace variations in intracellular P_i of producer and free P_i in the environment. In this paper, we develop a novel stoichiometric IGP model by explicitly tracking the P_i cell quota of producer and free P_i. Moreover, the effect of light on producer growth is explicitly considered in our model by utilizing the product of the Droop equation and the Monod equation. Our primary aim in developing this comprehensive model was to more precisely capture the growth responses of IG prey and IG predator to varying quality producers, thereby enhancing our comprehension of the influence of nutrient levels in the aquatic environment on IGP population dynamics.

The remainder of this paper is organized as follows. In section 2, we develop a novel stoichiometric IGP model by explicitly tracking the P_i cell quota of producer and free P_i. In section 3, we validate the model using experimental data of algae, ciliate, and *Daphnia* from the mesocosm experiment of Diehl et al (2022). The data fitting results demonstrate that our model adeptly replicates the behavior of these three species. In section 4, the well-posedness and dynamics of our model are studied. In section 5, we present the results of numerical simulations, exploring the influence of light intensity,

nutrient concentration, and the phosphorus-to-carbon ratio of IG prey on IGP model dynamics. Our findings are succinctly summarized in the last section.

2 Model derivation

In this section, we develop a stoichiometric algae-ciliate-*Daphnia* model with an intraguild predation structure by explicitly tracking free $\mathrm{P_i}$ in the environment and intracellular $\mathrm{P_i}$ in algae. Our model comprises five nonlinear differential equations that track variations in algal carbon density (A), ciliate carbon density (C), *Daphnia* carbon density (D), $\mathrm{P_i}$ cell quota of algae (Q), and $\mathrm{P_i}$ concentration in the aquatic environment (P_f). This model simulates a well-mixed system open only to light and air. A schematic diagram of the model is shown in Fig. 1.

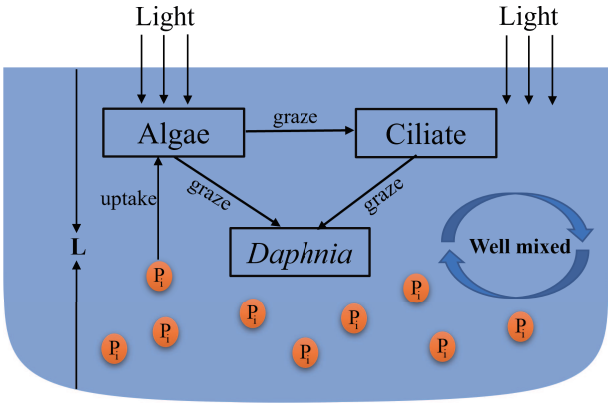

Fig. 1 Schematic diagram for our mathematical modeling.

Let P_a, P_c, and P_d describe the intracellular $\mathrm{P_i}$ of algae, ciliate, and *Daphnia*, respectively. Then $Q = P_a/A$ represents the $\mathrm{P_i}$ cell quota of algae. Since the phosphorus-to-carbon ratio of predators changes very little, here we assume that ciliate and *Daphnia* have fixed phosphorus to carbon ratio θ_1 and θ_2, respectively. Then one can obtain that $P_c = C\theta_1$ and $P_d = D\theta_2$. The following equation tracks the intracellular $\mathrm{P_i}$ of algae

$$\frac{\mathrm{d}P_a}{\mathrm{d}t} = \underbrace{u(P_f,Q)A}_{\text{Uptake by algae}} - \underbrace{\frac{P_a}{A}f(A)C}_{\text{Loss due to ciliate grazing}} - \underbrace{\frac{P_a}{A}g(A)D}_{\text{Loss due to } \textit{Daphnia} \text{ grazing}} - \underbrace{d_1P_a}_{\text{Loss due to death}}, \tag{1}$$

where $u(P_f, Q)$ is the $\mathrm{P_i}$ uptake rate of algae, which is regulated by both free $\mathrm{P_i}$ (P_f) and algal cell quota (Q). As P_f increases, the $\mathrm{P_i}$ uptake rate increases, and finally tends to a saturated value. On the contrary, as cell quota Q increases, the uptake rate gradually diminishes, reaching zero when it reaches the maximum cell quota Q_M. Therefore, the following equation can be used to describe the algal $\mathrm{P_i}$ uptake rate

(Diehl et al, 2005),

$$u(P_f, Q) = \frac{\gamma P_f}{(P_f + K_p)} \frac{(Q_M - Q)}{(Q_M - Q_m)},$$

where γ is the maximum P_i uptake rate of algae, K_p is the half-saturation constant for P_i uptake of algae, Q_M is the maximum P_i cell quota of algae, and Q_m is the minimum P_i cell quota of algae. The second and third items of (1) represent the loss of P_i in algal cells due to the graze of ciliate and *Daphnia*, respectively. The last item is the P_i loss due to algal death.

In the natural environment, the restriction of multiple nutrients and light on the algal growth is referred to as co-limitation (Arrigo, 2005). Previous studies have proposed two different forms of algal growth models that consider co-limitation: threshold model and multiplicative model (Lee et al, 2015). The threshold model, also known as Liebig's minimum law, assumes that the growth rate of algae is determined by the most limited resource among all the required resources for growth. This model is commonly used to describe the joint effects of multiple nutrients on the specific growth rate of algae, particularly the co-limitation of nitrogen and phosphorus (Guest et al, 2013). The multiplicative model assumes that all major resources can simultaneously affect algal growth rate, which is often employed to describe the collective constraints imposed by nutrients, temperature, pH, CO_2, and light intensity on algal growth (Wang et al, 2007; Yan et al, 2022; Chen et al, 2015).

When light enters the water, a portion of it is absorbed by suspended matter and phytoplankton in the water. The light intensity at the water depth d can be expressed by the classical Lambert-Beer law (Huisman and Weissing, 1994) as

$$I(d, A) = I_{in} \exp(-(kA + K_{bg})d), \quad 0 < d < L,$$

where $d = 0$ means the water surface, $d = L$ represents the bottom of the mixed layer, I_{in} is the light intensity on the water surface, k is the specific light attenuation coefficient of phytoplankton biomass, and K_{bg} is the background light attenuation coefficient.

Based on these considerations, we employ the multiplicative form of the Droop and Monod equations to describe the co-limitation of the P_i concentration and the intensity of light on algal growth. Thus, the specific algal growth rate μ can be represented as

$$\mu = \mu_{\max} \left(1 - \frac{Q_m}{Q}\right) \bar{I}(A),$$

where $\bar{I}(A) = \frac{1}{L}\int_0^L \frac{I(x,A)}{I(x,A)+h} dx = \frac{1}{L(kA+K_{bg})} \ln\left(\frac{h+I_{in}}{h+I(L,A)}\right)$ is the average light intensity in the water column (López Muñoz and Bernard, 2021; Guedes et al, 2023; Wang et al, 2007), $\mu_{\max}$ is the maximum growth rate of algae, and h is the half-saturation constant of light-dependent algal production. Note that $\bar{I}(A)$ is decreasing with respect to A. The loss of algal biomass is caused by cell death and graze, in which both ciliate and *Daphnia* are able to prey on algae. Therefore, the change rate of algal biomass

can be expressed as

$$\frac{\mathrm{d}A}{\mathrm{d}t} = \mu_{\max}\left(1 - \frac{Q_m}{Q}\right)\bar{I}(A)A - f(A)C - g(A)D - d_1 A, \tag{2}$$

where d_1 is the loss rate of algae, $f(A)$ and $g(A)$ are functional response functions, which describe the rate at which ciliate and *Daphnia* ingest algae, respectively.

Therefore, from equations (1) and (2) we can get the following equation to track changes in algae cell quota,

$$\frac{\mathrm{d}Q}{\mathrm{d}t} = u(P_f, Q) - \mu_{\max}\left(1 - \frac{Q_m}{Q}\right)\bar{I}(A)Q. \tag{3}$$

We then obtain the following stoichiometric algae-ciliate-*Daphnia* model with intraguild predation structure:

$$\begin{cases}
\dfrac{\mathrm{d}A}{\mathrm{d}t} = \underbrace{\mu_{\max}\left(1 - \dfrac{Q_m}{Q}\right)\bar{I}(A)A}_{\text{Algae growth}} - \underbrace{f(A)C}_{\text{Ciliate graze}} - \underbrace{g(A)D}_{\textit{Daphnia} \text{ graze}} - \underbrace{d_1 A}_{\text{Algae death}}, \\
\dfrac{\mathrm{d}C}{\mathrm{d}t} = \underbrace{e_1 \min\left\{1, \dfrac{Q}{\theta_1}\right\} f(A)C}_{\text{Growth limited by algae quality and quantity}} - \underbrace{h(C)D}_{\textit{Daphnia} \text{ graze}} - \underbrace{d_2 C}_{\text{Ciliate death}}, \\
\dfrac{\mathrm{d}D}{\mathrm{d}t} = \underbrace{e_2 \min\left\{1, \dfrac{Q}{\theta_2}\right\} g(A)D}_{\text{Growth limited by algae quality and quantity}} + \underbrace{e_3 \min\left\{1, \dfrac{\theta_1}{\theta_2}\right\} h(C)D}_{\text{Growth limited by ciliate quality and quantity}} \\
\qquad - \underbrace{d_3 D}_{\textit{Daphnia} \text{ death}}, \\
\dfrac{\mathrm{d}Q}{\mathrm{d}t} = \underbrace{u(P_f, Q)}_{\text{Phosphate uptake}} - \underbrace{\mu_{\max}\left(1 - \dfrac{Q_m}{Q}\right)\bar{I}(A)Q}_{\text{Phosphate dilution due to algae growth}}, \\
\dfrac{\mathrm{d}P_f}{\mathrm{d}t} = \underbrace{-u(P_f, Q)A}_{\text{P}_\text{i} \text{ consumption by algae}} + \underbrace{(Q - e_2 \min\{\theta_2, Q\})\, g(A)D + (\theta_1 - e_3 \min\{\theta_1, \theta_2\})\, h(C)D}_{\text{P}_\text{i} \text{ recycling from } \textit{Daphnia} \text{ feces}} \\
\qquad + \underbrace{(Q - e_1 \min\{\theta_1, Q\})f(A)C}_{\text{Phosphate recycling from ciliate feces}} + \underbrace{d_1 AQ}_{\text{Phosphate recycling from dead algae}} \\
\qquad + \underbrace{d_2 C\theta_1}_{\text{Phosphate recycling from dead ciliate}} + \underbrace{d_3 D\theta_2}_{\text{Phosphate recycling from dead } \textit{Daphnia}}.
\end{cases} \tag{4}$$

The units and biological meaning of all state variables and parameters of model (4) are shown in Tables 1 and 2. Given the biological significance of model (4), we assume that all parameter values are positive. The first term of the second equation of model (4), $e_1 \min\{1, Q/\theta_1\}$, is the growth efficiency of ciliate, which depends on the algal quality Q. If $Q > \theta_1$, then the ciliate converts the consumed algae with the maximum

Table 1 Model variables.

Variables	Meaning	Units
A	Algae carbon density	mg C/m^3
C	Ciliate carbon density	mg C/m^3
D	*Daphnia* carbon density	mg C/m^3
Q	P_i cell quota of algae	mg P_i/mg C
P_f	P_i concentration in the environment	mg P_i/m^3

Table 2 Model parameters.

Parameters	Meaning	Values	Units	Source
Q_M	Maximum P_i cell quota of algae	0.0398	mg P_i/mg C	(Diehl et al, 2022)
θ_1	phosphorus to carbon ratio of ciliate	0.0245	mg P_i/mg C	(Diehl et al, 2022)
θ_2	phosphorus to carbon ratio of *Daphnia*	0.0323	mg P_i/mg C	(Diehl et al, 2022)
L	Depth of the water column	1.5	m	(Diehl et al, 2022)
k	Specific light attenuation coefficient of algae	0.00036	m^2/mg C	(Diehl et al, 2022)
K_{bg}	Background light attenuation coefficient	1	m^{-1}	(Diehl et al, 2022)
I_{in}	Light intensity at water surface	240	µmol photons/(m$^2 \cdot$ s)	(Diehl et al, 2022)
h	Half-saturation constant of light-dependent algal production	120	µmol photons/(m$^2 \cdot$ s)	(Diehl et al, 2022)
$\mu_{\max}$	Maximum growth rate of algae	0.56	day^{-1}	Fitting
Q_m	Minimum P_i cell quota of algae	0.0001	mg P_i/mg C	Fitting
a_1	Half saturation constant of ciliate ingestion response to algae	725	mg C/m^3	Fitting
a_2	Half saturation constant of *Daphnia* ingestion response to algae	858	mg C/m^3	Fitting
a_3	Half saturation constant of *Daphnia* ingestion response to ciliate	212	mg C/m^3	Fitting
K_p	Half saturation constant for P_i uptake of algae	15.6	mg P_i/m^3	Fitting
σ_1	Maximal ingestion rate of ciliate on algae	0.76	day^{-1}	Fitting
σ_2	Maximal ingestion rate of *Daphnia* on algae	0.82	day^{-1}	Fitting
σ_3	Maximal ingestion rate of *Daphnia* on ciliate	0.75	day^{-1}	Fitting
γ	Maximum specific P_i uptake rate of algae	0.012	day^{-1}	Fitting
d_1	Algae death rate	0.18	day^{-1}	Fitting
d_2	Ciliate death rate	0.01	day^{-1}	Fitting
d_3	*Daphnia* death rate	0.105	day^{-1}	Fitting
e_1	Maximal production efficiency of ciliate from consuming algae	0.85		Fitting
e_2	Maximal production efficiency of *Daphnia* from consuming algae	0.68		Fitting
e_3	Maximal production efficiency of *Daphnia* from consuming ciliate	0.74		Fitting
r	Decomposition ratio of dead cells by microorganisms	0.5		Fitting

efficiency e_1 and egests the excessively ingested $\mathrm{P_i}$. If $Q < \theta_1$, it implies that ciliate is limited by $\mathrm{P_i}$, the efficiency is $e_1 Q/\theta_1$. Similarly, we utilize the minimum functions $e_2 \min\{1, Q/\theta_2\}$ and $e_3 \min\{1, \theta_1/\theta_2\}$ to describe the growth efficiency of *Daphnia* by consuming algae and ciliate, respectively. Notice that $e_i < 1, i = 1, 2, 3$ due to the second law of thermodynamics. In the last equation of model (4), $u(P_f, Q)A$ is the $\mathrm{P_i}$ uptake by algae, $d_1 AQ$, $d_2 C\theta_1$, and $d_3 D\theta_2$ are the $\mathrm{P_i}$ recycling from the dead cells of algae, ciliate, and *Daphnia*, respectively. $(Q - e_1 \min\{\theta_1, Q\}) f(A)C$ describes the $\mathrm{P_i}$ received by ciliate preying on algae minus the actual $\mathrm{P_i}$ retained due to growth and maintenance needs, this gives the amount of $\mathrm{P_i}$ recovered from ciliate manure and other losses. Similarly, $(Q - e_2 \min\{\theta_2, Q\})\, g(A)D$ and $(\theta_1 - e_3 \min\{\theta_1, \theta_2\})\, h(C)D$ are the amount of $\mathrm{P_i}$ recovered from *Daphnia* manure and other losses. Here, $h(C)$ is the functional response function, which describes the rate of *Daphnia* ingest ciliate. In this paper, we use the following Holling type II functional response functions (Holling, 1965):

$$f(A) = \frac{\sigma_1 A}{a_1 + A},\ g(A) = \frac{\sigma_2 A}{a_2 + A},\ h(C) = \frac{\sigma_3 C}{a_3 + C},$$

where σ_1 is the maximal ingestion rate of the ciliate on algae, σ_2 is the maximal ingestion rate of the *Daphnia* on algae, σ_3 is the maximal ingestion rate of the *Daphnia* on ciliate, a_1 is the half-saturation constant of the ciliate ingestion response to algae, a_2 is the half-saturation constant of the *Daphnia* ingestion response to algae, a_3 is the half-saturation constant of the *Daphnia* ingestion response to ciliate.

Let $P = AQ + C\theta_1 + D\theta_2 + P_f$ be the total $\mathrm{P_i}$ of the system. We can easily check that $\frac{\mathrm{d}P}{\mathrm{d}t} = 0$. Thus, the total $\mathrm{P_i}$ of model (4) is kept at a constant level, and then we can formulate an expression for the free $\mathrm{P_i}$, $P_f = P - AQ - C\theta_1 - D\theta_2$. Therefore, model (4) can be reduced to the following four equations:

$$\begin{cases} \dfrac{\mathrm{d}A}{\mathrm{d}t} = \underbrace{\mu_{\max}\left(1 - \dfrac{Q_m}{Q}\right)\bar{I}(A)A}_{\text{Algae growth}} - \underbrace{f(A)C}_{\text{Ciliate graze}} - \underbrace{g(A)D}_{\textit{Daphnia} \text{ graze}} - \underbrace{d_1 A}_{\text{Algae death}}, \\ \dfrac{\mathrm{d}C}{\mathrm{d}t} = \underbrace{e_1 \min\left\{1, \dfrac{Q}{\theta_1}\right\} f(A)C}_{\text{Growth limited by algae quality and quantity}} - \underbrace{h(C)D}_{\textit{Daphnia} \text{ graze}} - \underbrace{d_2 C}_{\text{Ciliate death}}, \\ \dfrac{\mathrm{d}D}{\mathrm{d}t} = \underbrace{e_2 \min\left\{1, \dfrac{Q}{\theta_2}\right\} g(A)D}_{\text{Growth limited by algae quality and quantity}} + \underbrace{e_3 \min\left\{1, \dfrac{\theta_1}{\theta_2}\right\} h(C)D}_{\text{Growth limited by ciliate quality and quantity}} - \underbrace{d_3 D}_{\textit{Daphnia} \text{ death}}, \\ \dfrac{\mathrm{d}Q}{\mathrm{d}t} = \underbrace{u(P - AQ - \theta_1 C - \theta_2 D, Q)}_{\text{Phosphate uptake}} - \underbrace{\mu_{\max}\left(1 - \dfrac{Q_m}{Q}\right)\bar{I}(A)Q}_{\text{Phosphate dilution due to algae growth}}. \end{cases} \tag{5}$$

3 Model validation

In this section, we validate model (4) using experimental data of algae, ciliate, and *Daphnia* from the mesocosm experiment conducted by Diehl et al (2022). Their experimental results showed a decreasing trend in the total P_i of the system during the experiment. This decline could be attributed to the low activity of microorganisms, leading to a slow decomposition rate of dead cells (algae, ciliate, and *Daphnia*). To account for the incomplete decomposition of these dead cells during the experiment, we introduce a decomposition ratio, denoted as r, when fitting the experimental data. Consequently, the last equation of model (4) can be modified as

$$\begin{aligned}\frac{\mathrm{d}P_f}{\mathrm{d}t} =& -u(P_f,Q)A + (Q - e_1\min\{\theta_1,Q\})f(A)C + (Q - e_2\min\{\theta_2,Q\})\,g(A)D \\ &+ (\theta_1 - e_3\min\{\theta_1,\theta_2\})\,h(C)D + r\left(d_1AQ + d_2C\theta_1 + d_3D\theta_2\right).\end{aligned}$$

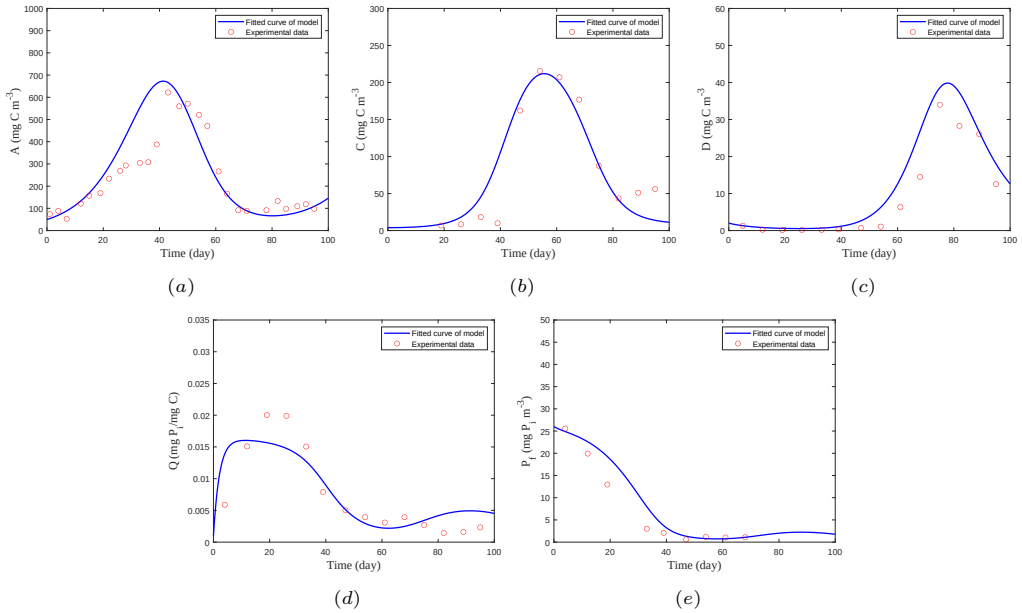

Fig. 2 Comparison of the fitted curves of model (4) with experimental data. (a) Algal carbon density (A); (b) Ciliate carbon density (C); (c) *Daphnia* carbon density (D); (d) P_i cell quota of algae (Q); (e) P_i concentration in the environment (P_f). The parameter values of model (4) can be estimated by fitting the five state variables simultaneously, and the parameter values are shown in Table 2.

Some parameter values of model (4) are determined according to the experimental conditions. The remaining parameter values are obtained by fitting the five variables of model (4) with the experimental data simultaneously using the least squares method, which is implemented with the "fmincon" function in MATLAB (R2020b). The estimated parameter values are given in Table 2. In addition, the model cost of all state

variables is calculated to assess the fitting accuracy of model (4), following the method described by Gao et al (2022). The fitting results show that the solution of model (4) can well capture the changes in experimental data, especially A and P_f have better fitting effects, and the model costs are 4.0854 and 5.1811 respectively (Fig. 2). The remaining variables, C, D, and Q, also capture the changing trend of the experimental data, with model costs of 80.8821, 67.5164, and 11.9871, respectively. The model validation results show that under appropriate parameter values, our model can accurately track the dynamics of the three populations of algae, ciliate, and *Daphnia*.

4 Qualitative analysis

In this section, we conduct a basic analysis of model (5), confirming the boundedness and positivity of the solution, establishing the existence of boundary equilibria, and investigating their stability. Furthermore, we demonstrate the existence of the positive equilibrium using the persistence theory (Zhao, 2003).

4.1 Well-posedness

The boundedness and positive invariance of the solution of model (5) can be guaranteed by the following theorem, which shows that model (5) is biologically well-defined.

Theorem 1. *Solutions of model* (5) *with initial conditions in the set*

$$\Delta = \left\{(A, C, D, Q)\middle| 0 < A,\ 0 < C,\ 0 < D,\ Q_m < Q < Q_M,\ AQ + \theta_1 C + \theta_2 D < P\right\}$$

will remain there for all forward time.

Proof. Let $S(t) = (A(t), C(t), D(t), Q(t))$ be a solution of model (5) with $S(0) \in \Delta$. Notice that $A = 0$, $C = 0$, and $D = 0$ are all solutions of model (5). Thus, by the theorem of existence and uniqueness of solutions, $S(t)$ cannot leave the region Δ by touching or crossing these boundary planes. Suppose that there exists a positive t_1 such that $S(t)$ touches or crosses the boundary of Δ for the first time. Then there must have three cases: $Q(t_1) = Q_m$ or $Q(t_1) = Q_M$ or $A(t_1)Q(t_1) + \theta_1 C(t_1) + \theta_2 D(t_1) = P$. In the following, we will show all these three cases are impossible using proof by contradiction.

Case 1. Assume that $A(t_1)Q(t_1) + \theta_1 C(t_1) + \theta_2 D(t_1) = P$. Denote

$$V = A(t)Q(t) + \theta_1 C(t) + \theta_2 D(t).$$

Then $V(t) < P$ for $t \in [0, t_1)$ and $V(t_1) = P$, which implies that $\frac{\mathrm{d}V}{\mathrm{d}t}\big|_{t=t_1} \geq 0$. On the other hand, along the solution of model (5) we can compute that

$$\begin{aligned}\frac{\mathrm{d}V}{\mathrm{d}t}\Big|_{t=t_1} =& A'(t_1)Q(t_1) + A(t_1)Q'(t_1) + \theta_1 C'(t_1) + \theta_2 D'(t_1)\\ \leq& \frac{\sigma_1 A(t_1)C(t_1)Q(t_1)}{a_1 + A(t_1)}(e_1 - 1) + \frac{\sigma_2 A(t_1)D(t_1)Q(t_1)}{a_2 + A(t_1)}(e_2 - 1)\\ &+ \frac{\theta_1\sigma_3 C(t_1)D(t_1)}{a_3 + C(t_1)}(e_3 - 1) - d_1 A(t_1)Q(t_1) - \theta_1 d_2 C(t_1) - \theta_2 d_3 D(t_1)\\ <& 0.\end{aligned}$$

A contradiction. Thus we can confirm that $A(t)Q(t) + \theta_1 C(t) + \theta_2 D(t) < P$ for all $t \geq 0$.

Case 2. Assume that $Q(t_1) = Q_m$. In this case, $Q_m < Q(t) < Q_M$ for $t \in [0, t_1)$, and therefore $\frac{\mathrm{d}Q}{\mathrm{d}t}\big|_{t=t_1} \leq 0$. On the other hand, by noticing from case 1 that $A(t_1)Q_m + \theta_1 C(t_1) + \theta_2 D(t_1) < P$, we have

$$\frac{\mathrm{d}Q}{\mathrm{d}t}\Big|_{t=t_1} = u(P - A(t_1)Q_m - \theta_1 C(t_1) - \theta_2 D(t_1), Q_m) > 0,$$

which, again, leads to a contradiction. Therefore $Q(t) > Q_m$ for all $t \geq 0$.

Case 3. If $Q(t_1) = Q_M$. Similar logic as that for case 2 we can prove $Q(t) < Q_M$ for all $t \geq 0$.

Summarizing above, we obtain that Δ is a positive invariant set of model (5). □

For the convenience of mathematical analysis, we rewrite model (5) as the following form:

$$\frac{\mathrm{d}A}{\mathrm{d}t} = AF(A, C, D, Q), \frac{\mathrm{d}C}{\mathrm{d}t} = CG(A, C, D, Q), \frac{\mathrm{d}D}{\mathrm{d}t} = DH(A, C, Q), \frac{\mathrm{d}Q}{\mathrm{d}t} = W(A, C, D, Q), \tag{6}$$

where

$$\begin{aligned}F(A, C, D, Q) =& \mu_{\max}\left(1 - \frac{Q_m}{Q}\right)\bar{I}(A) - \frac{\sigma_1 C}{a_1 + A} - \frac{\sigma_2 D}{a_2 + A} - d_1,\\ G(A, C, D, Q) =& e_1 \min\left\{1, \frac{Q}{\theta_1}\right\}\frac{\sigma_1 A}{a_1 + A} - \frac{\sigma_3 D}{a_3 + C} - d_2,\\ H(A, C, Q) =& e_2 \min\left\{1, \frac{Q}{\theta_2}\right\}\frac{\sigma_2 A}{a_2 + A} + e_3 \min\left\{1, \frac{\theta_1}{\theta_2}\right\}\frac{\sigma_3 C}{a_3 + C} - d_3,\\ W(A, C, D, Q) =& \frac{\gamma(P - AQ - \theta_1 C - \theta_2 D)(Q_M - Q)}{(P - AQ - \theta_1 C - \theta_2 D + K_p)(Q_M - Q_m)} - \mu_{\max}\left(1 - \frac{Q_m}{Q}\right)\bar{I}(A)Q.\end{aligned}$$

4.2 Boundary equilibria

Model (5) may exist the following four types of boundary equilibria:

(i) Total extinction equilibrium $E_0 = (0, 0, 0, \hat{Q})$, where

$$\hat{Q} = \frac{\gamma P Q_M + \mu_{\max} Q_m \bar{I}(0)(P + K_p)(Q_M - Q_m)}{\gamma P + \mu_{\max} \bar{I}(0)(P + K_p)(Q_M - Q_m)}. \tag{7}$$

(ii) Algae-only equilibrium $E_1 = (A_1, 0, 0, Q_1)$, where $Q_1 = \frac{\mu_{\max} \bar{I}(A_1) Q_m}{\mu_{\max} \bar{I}(A_1) - d_1}$ and A_1 is the positive root of the equation

$$\frac{\gamma(P - AQ_1)(Q_M - Q_1)}{(P - AQ_1 + K_p)(Q_M - Q_m)} - d_1 \frac{\mu_{\max} \bar{I}(A) Q_m}{\mu_{\max} \bar{I}(A) - d_1} = 0. \tag{8}$$

(iii) *Daphnia*-absent equilibrium $E_2 = (A_2, C_2, 0, Q_2)$, where

$$A_2 = \frac{a_1 d_2}{e_1 \min\left\{1, \frac{Q_2}{\theta_1}\right\} \sigma_1 - d_2}, \; C_2 = \left(\mu_{\max}\Big(1 - \frac{Q_m}{Q_2}\Big) \bar{I}(A_2) - d_1\right) \frac{a_1 + A_2}{\sigma_1},$$

and Q_2 is the positive root of the equation

$$\frac{\gamma(P - A_2 Q - C_2 \theta_1)}{P - A_2 Q - C_2 \theta_1 + K_p} \frac{Q_M - Q}{Q_M - Q_m} - \left(d_1 + \frac{\sigma_1 C_2}{a_1 + A_2}\right) Q = 0. \tag{9}$$

(iv) Ciliate-absent equilibrium $E_3 = (A_3, 0, D_3, Q_3)$, where

$$A_3 = \frac{a_2 d_3}{e_2 \min\left\{1, \frac{Q_3}{\theta_2}\right\} \sigma_2 - d_3}, \; D_3 = \left(\mu_{\max}\Big(1 - \frac{Q_m}{Q_3}\Big) \bar{I}(A_3) - d_1\right) \frac{a_2 + A_3}{\sigma_2},$$

and Q_3 is the positive root of the equation

$$\frac{\gamma(P - A_3 Q - D_3 \theta_2)}{P - A_3 Q - D_3 \theta_2 + K_p} \frac{Q_M - Q}{Q_M - Q_m} - \left(d_1 + \frac{\sigma_2 D_3}{a_2 + A_3}\right) Q = 0. \tag{10}$$

Define

$$R_0 = \frac{\mu_{\max}\left(1 - \frac{Q_m}{\hat{Q}}\right) \bar{I}(0)}{d_1}, R_1^C = \frac{e_1 \min\left\{1, \frac{Q_1}{\theta_1}\right\} \frac{\sigma_1 A_1}{a_1 + A_1}}{d_2}, R_1^D = \frac{e_2 \min\left\{1, \frac{Q_1}{\theta_2}\right\} \frac{\sigma_2 A_1}{a_2 + A_1}}{d_3},$$

$$R_2^D = \frac{e_2 \min\left\{1, \frac{Q_2}{\theta_2}\right\} \frac{\sigma_2 A_2}{a_2 + A_2} + e_3 \min\{1, \frac{\theta_1}{\theta_2}\} \frac{\sigma_3 C_2}{a_3 + C_2}}{d_3}, R_3^C = \frac{e_1 \min\left\{1, \frac{Q_3}{\theta_1}\right\} \frac{\sigma_1 A_3}{a_1 + A_3} - \frac{\sigma_3 D_3}{a_3}}{d_2}.$$

Biologically, R_0 is called the ecological reproductive index of algae, which determines the invasion of the aquatic ecosystem by algae; R_1^C and R_3^C are two critical values determining respectively the invasion of the system by ciliate in the absence and presence of *Daphnia*; R_1^D and R_2^D are critical values determining respectively the invasion of the system by *Daphnia* in the absence and presence of ciliate.

The following theorems establish the existence of four-type boundary equilibria.

Theorem 2. *Model (5) always exists the total extinction equilibrium $E_0 = (0, 0, 0, \hat{Q})$, which is the only equilibrium if $R_0 < 1$. When $R_0 > 1$, model (5) exists a unique algae-only equilibrium $E_1 = (A_1, 0, 0, Q_1)$.*

Proof. Obviously, model (5) always exists the total extinction equilibrium $E_0 = (0, 0, 0, \hat{Q})$, where $\hat{Q}$ is defined in (7). Any algae-only equilibrium of model (5), if exists, must simultaneously satisfy $F(A, 0, 0, Q) = 0$ and $W(A, 0, 0, Q) = 0$, i.e., $Q = \frac{\mu_{\max}\bar{I}(A)Q_m}{\mu_{\max}\bar{I}(A)-d_1}$ and $\frac{\gamma(P-AQ)(Q_M-Q)}{(P-AQ+K_p)(Q_M-Q_m)} - d_1 Q = 0$. Define

$$f_1(A) = \frac{\mu_{\max}\bar{I}(A)Q_m}{\mu_{\max}\bar{I}(A) - d_1} \quad \text{and} \quad f_2(A) = \frac{\gamma(P - Af_1(A))(Q_M - f_1(A))}{(P - Af_1(A) + K_p)(Q_M - Q_m)}.$$

By simple calculations, one can obtain that

$$\begin{aligned}
\frac{\mathrm{d}f_1(A)}{\mathrm{d}A} &= -\frac{d_1\mu_{\max}\bar{I}'(A)Q_m}{(\mu_{\max}\bar{I}(A) - d_1)^2} > 0, \\
\frac{\mathrm{d}f_2(A)}{\mathrm{d}A} &= -\frac{\gamma K_p\left(f_1(A) + A\frac{\mathrm{d}f_1(A)}{\mathrm{d}A}\right)(Q_M - f_1(A))}{(P - Af_1(A) + K_p)^2(Q_M - Q_m)} - \frac{\gamma(P - Af_1(A))\frac{\mathrm{d}f_1(A)}{\mathrm{d}A}}{(P - Af_1(A) + K_p)(Q_M - Q_m)} < 0.
\end{aligned} \tag{11}$$

Thus, $f_1(A)$ and $f_2(A)$ are respectively monotonically increasing and decreasing with respect to A.

If $R_0 < 1$, then one can obtain that $\mu_{\max}\left(1 - \frac{Q_m}{\hat{Q}}\right)\bar{I}(0) < d_1$, and thus $\hat{Q} < \frac{\mu_{\max}\bar{I}(0)Q_m}{\mu_{\max}\bar{I}(0)-d_1} = f_1(0)$. Moreover, we can compute that

$$f_2(0) = \frac{\gamma P}{P + K_p}\frac{Q_M - f_1(0)}{Q_M - Q_m} < \frac{\gamma P}{P + K_p}\frac{Q_M - \hat{Q}}{Q_M - Q_m} = \mu_{\max}\left(1 - \frac{Q_m}{\hat{Q}}\right)\bar{I}(0)\hat{Q} < d_1 f_1(0).$$

Therefore $f_2(A) = d_1 f_1(A)$ has no positive root, which implies that model (5) does not exist the algae-only equilibrium.

If $R_0 > 1$, we have $\mu_{\max}\left(1 - \frac{Q_m}{\hat{Q}}\right)\bar{I}(0) > d_1$ and $\hat{Q} > \frac{\mu_{\max}\bar{I}(0)Q_m}{\mu_{\max}\bar{I}(0)-d_1} = f_1(0)$. Then, one can obtain

$$f_2(0) = \frac{\gamma P}{P + K_p}\frac{Q_M - f_1(0)}{Q_M - Q_m} > \frac{\gamma P}{P + K_p}\frac{Q_M - \hat{Q}}{Q_M - Q_m} = \mu_{\max}\left(1 - \frac{Q_m}{\hat{Q}}\right)\bar{I}(0)\hat{Q} > d_1 f_1(0).$$

Notice that any equilibrium of model (5) must lie in $\overline{\Delta}$, the closure of Δ. Define

$$\tilde{A}_1 = \min\{A | P - Af_1(A) = 0 \text{ or } Q_M - f_1(A) = 0\}.$$

Then $f_2(\tilde{A}_1) = 0$. Noticing also the monotonicity of $f_1(A)$ and $f_2(A)$, we must have $d_1 f_1(\tilde{A}_1) > f_2(\tilde{A}_1) = 0$. Therefore there must exist one unique positive $A_1 \in (0, \tilde{A}_1)$ such that $f_2(A_1) = d_1 f_1(A_1)$. This means that model (5) exists a unique algae-only equilibrium $E_1 = (A_1, 0, 0, Q_1)$ if $R_0 > 1$, where $Q_1 = \frac{\mu_{\max}\bar{I}(A_1)Q_m}{\mu_{\max}\bar{I}(A_1)-d_1}$. □

Theorem 3. *If* $\min\{R_0, R_1^C\} > 1$*, then model* (5) *has at least one* Daphnia*-absent equilibrium* $E_2 = (A_2, C_2, 0, Q_2)$*. Moreover, if* $\theta_1 < Q_m$*,* E_2 *is unique.*

Proof. By solving $F(A, C, 0, Q) = 0$, $G(A, C, 0, Q) = 0$, and $W(A, C, 0, Q) = 0$, we obtain that

$$A = \frac{a_1 d_2}{e_1 \min\left\{1, \frac{Q}{\theta_1}\right\}\sigma_1 - d_2} := g_1(Q), \tag{12}$$

$$C = \left(\mu_{\max}\left(1 - \frac{Q_m}{Q}\right)\bar{I}(A) - d_1\right)\frac{a_1 + A}{\sigma_1} := g_2(Q) \tag{13}$$

and

$$\frac{\gamma(P - AQ - \theta_1 C)(Q_M - Q)}{(P - AQ - \theta_1 C + K_p)(Q_M - Q_m)} - \left(d_1 + \frac{\sigma_1 C}{a_1 + A}\right)Q = 0.$$

Notice from $G(A, C, 0, Q) = 0$ that $e_1 \min\left\{1, \frac{Q}{\theta_1}\right\}\sigma_1 - d_2 > 0$, and therefore $A = g_1(Q) > 0$. Define

$$G_1(Q) = \frac{\gamma(P - g_1(Q)Q - g_2(Q)\theta_1)(Q_M - Q)}{(P - g_1(Q)Q - g_2(Q)\theta_1 + K_p)(Q_M - Q_m)},\ G_2(Q) = \left(d_1 + \frac{\sigma_1 g_2(Q)}{a_1 + g_1(Q)}\right)Q.$$

Let $\tilde{Q}_2$ be the solution of $g_2(Q) = 0$, then we have

$$\mu_{\max}\left(1 - \frac{Q_m}{\tilde{Q}_2}\right)\bar{I}(g_1(\tilde{Q}_2)) = d_1. \tag{14}$$

Obviously, $\tilde{Q}_2 > Q_m$. Notice that $A = g_1(Q)$ and $\bar{I}(A)$ are decreasing with respect to Q and A, respectively. Thus $\bar{I}(g_1(Q))$ is increasing with Q, and hence $g_2(Q) > 0$ for $Q > \tilde{Q}_2$.

If $R_1^C > 1$, we assert that $\tilde{Q}_2 < Q_1$. In fact, from $R_1^C > 1$ we have that

$$A_1 > \frac{a_1 d_2}{e_1 \min\left\{1, \frac{Q_1}{\theta_1}\right\}\sigma_1 - d_2} = g_1(Q_1).$$

Assume that $\tilde{Q}_2 \geq Q_1$, then one can obtain that $g_1(\tilde{Q}_2) \leq g_1(Q_1) < A_1$ and therefore $\bar{I}(g_1(\tilde{Q}_2)) > \bar{I}(A_1)$. Thus, we have

$$\mu_{\max}\left(1 - \frac{Q_m}{\tilde{Q}_2}\right)\bar{I}(g_1(\tilde{Q}_2)) > \mu_{\max}\left(1 - \frac{Q_m}{Q_1}\right)\bar{I}(A_1) = d_1,$$

which contradicts with equation (14).

Notice that $G_1(Q_M) = 0 < G_2(Q_M)$. Therefore, if $G_1(\tilde{Q}_2) > G_2(\tilde{Q}_2)$, then $G_1(Q) = G_2(Q)$ has at least one positive root in $(\tilde{Q}_2, Q_M)$. From Theorem 2 we know that if $R_0 > 1$, E_1 exists and satisfies the following equations:

$$\mu_{\max}\left(1 - \frac{Q_m}{Q_1}\right)\bar{I}(A_1) = d_1 \text{ and } \frac{\gamma(P - A_1 Q_1)(Q_M - Q_1)}{(P - A_1 Q_1 + K_p)(Q_M - Q_m)} = \mu_{\max}\left(1 - \frac{Q_m}{Q_1}\right)\bar{I}(A_1)Q_1. \tag{15}$$

From equations (14) and (15) we have $\bar{I}(A_1) < \bar{I}(g_1(\tilde{Q}_2))$, which implies that $g_1(\tilde{Q}_2) < A_1$. Therefore, one can obtain that

$$G_1(\tilde{Q}_2) = \frac{\gamma(P - g_1(\tilde{Q}_2)\tilde{Q}_2)(Q_M - \tilde{Q}_2)}{(P - g_1(\tilde{Q}_2)\tilde{Q}_2 + K_p)(Q_M - Q_m)} > \frac{\gamma(P - A_1Q_1)(Q_M - Q_1)}{(P - A_1Q_1 + K_p)(Q_M - Q_m)} > d_1\tilde{Q}_2 = G_2(\tilde{Q}_2),$$

where we have used equation (15) in the last inequality. Thus, $G_1(Q) = G_2(Q)$ has at least one positive root $Q_2 \in (\tilde{Q}_2, Q_M)$, which implies that model (5) has at least one equilibrium $E_2 = (A_2, C_2, 0, Q_2)$ if $\min\{R_0, R_1^C\} > 1$, where A_2 and C_2 can be calculated from (12) and (13), respectively.

Moreover, if $\theta_1 < Q_m$, then $A_2 = \frac{a_1 d_2}{e_1\sigma_1 - d_2}$ and

$$C_2 = \left(\mu_{\max}(1 - \frac{Q_m}{Q_2})\bar{I}(A_2) - d_1\right)\frac{a_1 + A_2}{\sigma_1}.$$

By simple calculations, one can obtain that $G_1(Q)$ and $G_2(Q)$ are monotonically decreasing and increasing with respect to Q, respectively. Therefore, in combination with the above analyses, we can conclude that $G_1(Q) = G_2(Q)$ has a unique positive root $Q_2 \in (\tilde{Q}_2, Q_M)$. That is to say, model (5) exists one unique equilibrium E_2 if $\min\{R_0, R_1^C\} > 1$ and $\theta_1 < Q_m$ hold. □

Theorem 4. *If* $\min\{R_0, R_1^D\} > 1$, *then model* (5) *has at least one ciliate-absent equilibrium* $E_3 = (A_3, 0, D_3, Q_3)$. *Moreover, if* $\theta_2 < Q_m$, E_3 *is unique.*

The proof of Theorem 4 is similar to that of Theorem 3, we omit it.

4.3 Stability of boundary equilibria

The following theorems give the local and global asymptotic stability properties of the four-type boundary equilibria.

Theorem 5. *The total extinction equilibrium* E_0 *is locally asymptotically stable if* $R_0 < 1$, *while it is unstable if* $R_0 > 1$. *Moreover,* E_0 *is globally asymptotically stable if* $\hat{R}_0 = \frac{\mu_{\max}\left(1 - \frac{Q_m}{Q_M}\right)\bar{I}(0)}{d_1} < 1$.

The proof can be found in Appendix A.

Theorem 6. *Assume that* $R_0 > 1$. *If* $\max\left\{R_1^C, R_1^D\right\} < 1$, *the algae-only equilibrium* E_1 *is locally asymptotically stable, while it is unstable if* $\max\left\{R_1^C, R_1^D\right\} > 1$. *Moreover, if*

$$\hat{R}_1^C = \frac{e_1\sigma_1 \min\left\{1, \frac{Q_M}{\theta_1}\right\}}{d_2} < 1 \quad \textit{and} \quad \hat{R}_1^D = \frac{e_2\sigma_2 \min\left\{1, \frac{Q_M}{\theta_2}\right\}}{d_3} < 1,$$

then E_1 *is globally asymptotically stable.*

The proof can be found in Appendix B.

Theorem 7. *Assume that* $\min\{R_0, R_1^C\} > 1$. *If* $R_2^D > 1$, *the* Daphnia*-absent equilibrium* E_2 *is unstable. When* $R_2^D < 1$, E_2 *is locally asymptotically stable if one of the following conditions hold:*

(i) $Q_2 > \theta_1$ *and* $d_1 > d_1^* := \mu_{\max}\left(1 - \frac{Q_m}{Q_2}\right)\left(\bar{I}'(A_2)\left(1 - \frac{Q_m}{Q_2}\right)(a_1 + A_2) + \bar{I}(A_2)\right)$;

(ii) $Q_2 < \theta_1$, $d_1 > d_1^{**} := \mu_{\max}\Big(1-\frac{Q_m}{Q_2}\Big)\Big(\bar{I}'(A_2)\Big(a_1+A_2-\frac{e_1Q_2\sigma_1}{\theta_1}\Big)+\bar{I}(A_2)\Big)$, *and* $a_{21}a_{44} < a_{24}a_{41}$, *where* $a_{21} = C_2G_A(A_2,C_2,0,Q_2)$, $a_{24} = C_2G_Q(A_2,C_2,0,Q_2)$, $a_{41} = W_A(A_2,C_2,0,Q_2)$ *and* $a_{44} = W_Q(A_2,C_2,0,Q_2)$.

The proof can be found in Appendix C.

Theorem 8. *Assume that* $\min\{R_0, R_1^D\} > 1$. *If* $R_3^C > 1$, *then the ciliate-absent equilibrium* E_3 *is unstable. When* $R_3^C < 1$, *then* E_3 *is locally asymptotically stable if one of the following conditions hold.*

(i) $Q_3 > \theta_2$ *and* $d_1 > \mu_{\max}\left(1-\frac{Q_m}{Q_3}\right)\left(\bar{I}'(A_3)\left(1-\frac{Q_m}{Q_3}\right)(a_1+A_3)+\bar{I}(A_3)\right)$;

(ii) $Q_3 < \theta_2$, $d_1 > \mu_{\max}\Big(1-\frac{Q_m}{Q_3}\Big)\Big(\bar{I}'(A_3)\Big(a_2+A_3-\frac{e_2Q_3\sigma_2}{\theta_2}\Big)+\bar{I}(A_3)\Big)$, *and* $a_{31}a_{44} < a_{41}a_{34}$;

where $a_{31} = D_3H_A(A_3,0,D_3,Q_3)$, $a_{34} = D_3H_Q(A_3,0,D_3,Q_3)$, $a_{41} = W_A(A_3,0,D_3,Q_3)$, *and* $a_{44} = W_Q(A_3,0,D_3,Q_3)$.

The proof of Theorem 8 is similar to that of Theorem 7, we omit it.

Based on the above analyses, the existence and local stability of boundary equilibrium of model (5) can be summarized in Table 3.

Table 3 Existence and local stability of boundary equilibria of model (5)

Equilibria	Existence	Local stability
E_0	always exists	$R_0 < 1$
E_1	$R_0 > 1$	$R_1^C < 1, R_1^D < 1$
E_2	$R_0 > 1, R_1^C > 1$	$R_2^D < 1$, condition (i) or (ii) of Theorem 7 holds
E_3	$R_0 > 1, R_1^D > 1$	$R_3^C < 1$, condition (i) or (ii) of Theorem 8 holds

Remark 1. *It can be seen from the results of Theorems 5 to 8 that when the ecological reproduction index* (R_0) *of algae is less than 1, the algae cannot survive, and thus the ciliate and* Daphnia *will also become extinct. When* $R_0 > 1$, *algae can successfully invade the system, and if* $\max\{R_1^C, R_1^D\} < 1$, *then only algae exist in the system, otherwise ciliate or* Daphnia *can invade the system. If* $R_1^C > 1$, *then ciliate can invade the system containing only algae, and if* $R_2^D < 1$, *algae and ciliate can coexist but* Daphnia *become extinct. Similarly, if* $R_1^D < 1$, Daphnia *can invade the system containing only algae, and if* $R_3^C < 1$, Daphnia *and algae can coexist, and ciliate will become extinct.*

4.4 Interior equilibria

In this subsection, we explore the existence of interior equilibrium $E^* = (A^*, C^*, D^*, Q^*)$ by utilizing the persistence method (Zhao, 2003).

We first consider the following two subsystems: algae-ciliate subsystem

$$\begin{aligned}\frac{\mathrm{d}A}{\mathrm{d}t} =&\mu_{\max}\left(1-\frac{Q_m}{Q}\right)\bar{I}(A)A-\frac{\sigma_1 AC}{a_1+A}-d_1A,\\ \frac{\mathrm{d}C}{\mathrm{d}t} =&e_1\min\left\{1,\frac{Q}{\theta_1}\right\}\frac{\sigma_1 AC}{a_1+A}-d_2C,\\ \frac{\mathrm{d}Q}{\mathrm{d}t} =&\frac{\gamma(P-AQ-\theta_1C)(Q_M-Q)}{(P-AQ-\theta_1C+K_p)(Q_M-Q_m)}-\mu_{\max}\left(1-\frac{Q_m}{Q}\right)\bar{I}(A)Q,\end{aligned}\tag{16}$$

and algae-*Daphnia* subsystem

$$\begin{aligned}\frac{\mathrm{d}A}{\mathrm{d}t} =&\mu_{\max}\left(1-\frac{Q_m}{Q}\right)\bar{I}(A)A-\frac{\sigma_2 AD}{a_2+A}-d_1A,\\ \frac{\mathrm{d}D}{\mathrm{d}t} =&e_2\min\left\{1,\frac{Q}{\theta_2}\right\}\frac{\sigma_2 AD}{a_2+A}-d_3D,\\ \frac{\mathrm{d}Q}{\mathrm{d}t} =&\frac{\gamma(P-AQ-\theta_2D)(Q_M-Q)}{(P-AQ-\theta_2D+K_p)(Q_M-Q_m)}-\mu_{\max}\left(1-\frac{Q_m}{Q}\right)\bar{I}(A)Q.\end{aligned}\tag{17}$$

From Theorem 1, one can obtain that

$$\begin{aligned}\Delta_2 =&\{(A,C,Q)|0<A,\ 0<C,\ Q_m<Q<Q_M,\ AQ+\theta_1C<P\},\\ \Delta_3 =&\{(A,D,Q)|0<A,\ 0<D,\ Q_m<Q<Q_M,\ AQ+\theta_2D<P\}\end{aligned}$$

are the global attracting region and positive invariant set of model (16) and model (17), respectively.

To study the existence of E^*, we assume that $\Phi(t):\Delta\to\Delta$ is the solution semiflow of model (5). Let

$$\partial\Delta=\{(A,C,D,Q)\in\Delta|A=0 \text{ or } C=0 \text{ or } D=0, \text{ and } Q_m<Q<Q_M\}.$$

From Theorem 1, $\Phi(t)$ is point dissipative and compact and has a global attractor.

We introduce projections $X_i:\mathbb{R}^3_+\to\mathbb{R}_+, i=1,2,3$ and $Y_j:\mathbb{R}^3_+\to\mathbb{R}_+, j=1,2,3$ by

$$\begin{aligned}X_1(A,C,Q)=A,\ X_2(A,C,Q)=C,\ X_3(A,C,Q)=Q,\\ Y_1(A,D,Q)=A,\ Y_2(A,D,Q)=D,\ Y_3(A,D,Q)=Q.\end{aligned}$$

Let

$$\chi_1=X_1(\Delta_2),\ \chi_2=X_2(\Delta_2),\ \chi_3=X_3(\Delta_2),\ \psi_1=Y_1(\Delta_3),\ \psi_2=Y_2(\Delta_3),\ \psi_3=Y_3(\Delta_3),$$

and

$$\tilde{A}=\inf\chi_1,\ \tilde{C}=\inf\chi_2,\ \tilde{Q}=\inf\chi_3,\ \bar{A}=\inf\psi_1,\ \check{D}=\sup\psi_2,\ \bar{Q}=\inf\psi_3.$$

Define

$$\hat{R}_2^D = \frac{e_2 \min\left\{1, \frac{\tilde{Q}}{\theta_2}\right\} \frac{\sigma_2 \tilde{A}}{a_2+\tilde{A}} + e_3 \min\left\{1, \frac{\theta_1}{\theta_2}\right\} \frac{\sigma_3 \tilde{C}}{a_3+\tilde{C}}}{d_3} \text{ and } \hat{R}_3^C = \frac{e_1 \min\left\{1, \frac{\bar{Q}}{\theta_1}\right\} \frac{\sigma_1 \bar{A}}{a_1+\bar{A}} - \frac{\sigma_3 \check{D}}{a_3}}{d_2}.$$

Denote $M_1 = \{(A, C, 0, Q) | (A, C, Q) \in \Delta_2\}$ and $M_2 = \{(A, 0, D, Q) | (A, D, Q) \in \Delta_3\}$. Now we prove E_0, E_1, M_1, and M_2 are uniformly weak repellers with respect to Δ, i.e., there exists $\delta_i, i = 1, 2, 3, 4$ such that

$$\limsup_{t\to\infty} \operatorname{dist}(\Phi(t)q_0, E_0) \geq \delta_1, \limsup_{t\to\infty} \operatorname{dist}(\Phi(t)q_0, E_1) \geq \delta_2,$$
$$\limsup_{t\to\infty} \operatorname{dist}(\Phi(t)q_0, M_1) \geq \delta_3, \limsup_{t\to\infty} \operatorname{dist}(\Phi(t)q_0, M_2) \geq \delta_4,$$

for all $q_0 = (A_0, C_0, D_0, Q_0) \in \Delta$.

Lemma 9. *(i) If $R_0 > 1$, then E_0 is a uniform weak repeller for Δ;*
(ii) If $R_0 > 1$ and $\max\{R_1^C, R_1^D\} > 1$, then E_1 is a uniform weak repeller for Δ;
(iii) If $R_0 > 1$ and $\hat{R}_2^D > 1$, then M_1 is a uniform weak repeller for Δ;
(iv) If $R_0 > 1$ and $\hat{R}_3^C > 1$, then M_2 is a uniform weak repeller for Δ;

Proof. If $R_0 > 1$, $\max\{R_1^C, R_1^D\} > 1$, $\hat{R}_2^D > 1$, and $\hat{R}_3^C > 1$, then one can obtain that

$$\frac{\mu_{\max}\left(1 - \frac{Q_m}{\bar{Q}-\varepsilon}\right) \bar{I}(\varepsilon) - \frac{\sigma_1 \varepsilon}{a_1} - \frac{\sigma_2 \varepsilon}{a_2}}{d_1} > 1, \tag{18a}$$

$$\max\left\{ \frac{e_1 \min\left\{1, \frac{Q_1-\varepsilon}{\theta_1}\right\} \frac{\sigma_1(A_1-\varepsilon)}{a_1+A_1-\varepsilon} - \frac{\sigma_3 \varepsilon}{a_3}}{d_2}, \frac{e_2 \min\left\{1, \frac{Q_1-\varepsilon}{\theta_2}\right\} \frac{\sigma_2(A_1-\varepsilon)}{a_2+A_1-\varepsilon}}{d_3} \right\} > 1, \tag{18b}$$

$$\frac{e_2 \min\left\{1, \frac{\tilde{Q}-\varepsilon}{\theta_2}\right\} \frac{\sigma_2(\tilde{A}-\varepsilon)}{a_2+\tilde{A}-\varepsilon} + e_3 \min\{1, \frac{\theta_1}{\theta_2}\} \frac{\sigma_3(\tilde{C}-\varepsilon)}{a_3+\tilde{C}-\varepsilon}}{d_3} > 1, \tag{18c}$$

$$\frac{e_1 \min\left\{1, \frac{\bar{Q}-\varepsilon}{\theta_1}\right\} \frac{\sigma_1(\bar{A}-\varepsilon)}{a_1+\bar{A}-\varepsilon} - \frac{\sigma_3(\check{D}+\varepsilon)}{a_3}}{d_2} > 1, \tag{18d}$$

for a sufficiently small $\varepsilon > 0$.

Now we use the proof by contradiction to prove this Lemma. If the Lemma does not hold, then there are $q_i \in \Delta, i = 1, 2, 3, 4$ such that

$$\limsup_{t\to\infty} \operatorname{dist}(\Phi(t)q_1, E_0) < \varepsilon, \ \limsup_{t\to\infty} \operatorname{dist}(\Phi(t)q_2, E_1) < \varepsilon,$$
$$\limsup_{t\to\infty} \operatorname{dist}(\Phi(t)q_3, M_1) < \varepsilon, \ \limsup_{t\to\infty} \operatorname{dist}(\Phi(t)q_4, M_2) < \varepsilon,$$

here $\varepsilon > 0$ is defined as above. Thus, we can find $T_i, i = 1, 2, 3, 4$, such that

$$|A(t, q_1)| < \varepsilon, \ |C(t, q_1)| < \varepsilon, \ |D(t, q_1)| < \varepsilon, \ |Q(t, q_1) - \hat{Q}| < \varepsilon, \ t > T_1, \tag{19a}$$

$$|A(t,q_2)-A_1|<\varepsilon,\ |C(t,q_2)|<\varepsilon,\ |D(t,q_2)|<\varepsilon,\ |Q(t,q_2)-Q_1|<\varepsilon,\ t>T_2, \quad (19b)$$

$$\mathrm{dist}(A(t,q_3),\chi_1)<\varepsilon,\ \mathrm{dist}(C(t,q_3),\chi_2)<\varepsilon,\ |D(t,q_3)|<\varepsilon,\ \mathrm{dist}(Q(t,q_3),\chi_3)<\varepsilon,\ t>T_3, \quad (19c)$$

$$\mathrm{dist}(A(t,q_4),\psi_1)<\varepsilon,\ |C(t,q_4)|<\varepsilon,\ \mathrm{dist}(D(t,q_4),\psi_3)<\varepsilon,\ \mathrm{dist}(Q(t,q_3),\psi_3)<\varepsilon,\ t>T_4. \quad (19d)$$

From the first equation of model (5), we have

$$\frac{\mathrm{d}A(t,q_1)}{\mathrm{d}t}\geq\left(\mu_{\max}\left(1-\frac{Q_m}{\hat{Q}-\varepsilon}\right)\bar{I}(\varepsilon)-\frac{\sigma_1\varepsilon}{a_1}-\frac{\sigma_2\varepsilon}{a_2}-d_1\right)A,\quad t>T_1,$$

if (19a) holds. This means that $\limsup_{t\to\infty}A(t,q_1)=\infty$ since (18a) holds, which contradicts with (19a). Thus, (i) holds.

If (19b) holds, then one can obtain that

$$\frac{\mathrm{d}C(t,q_2)}{\mathrm{d}t}\geq\left(e_1\min\left\{1,\frac{Q_1-\varepsilon}{\theta_1}\right\}\frac{\sigma_1(A_1-\varepsilon)}{a_1+A_1-\varepsilon}-\frac{\sigma_3\varepsilon}{a_3}-d_2\right)C,\quad t>T_2,$$
$$\frac{\mathrm{d}D(t,q_2)}{\mathrm{d}t}\geq\left(e_2\min\left\{1,\frac{Q_1-\varepsilon}{\theta_2}\right\}\frac{\sigma_2(A_1-\varepsilon)}{a_2+A_1-\varepsilon}-d_3\right)D,\quad t>T_2,$$

which implies that $\limsup_{t\to\infty}C(t,q_2)=\infty$ or $\limsup_{t\to\infty}D(t,q_2)=\infty$ since (18b) holds. A contradiction with (19b), and then (ii) holds.

If (19c) holds, then

$$\frac{\mathrm{d}D(t,q_3)}{\mathrm{d}t}\geq\left(e_2\min\left\{1,\frac{\tilde{Q}-\varepsilon}{\theta_2}\right\}\frac{\sigma_2(\tilde{A}-\varepsilon)}{a_2+\tilde{A}-\varepsilon}+e_3\min\left\{1,\frac{\theta_1}{\theta_2}\right\}\frac{\sigma_3(\tilde{C}-\varepsilon)}{a_3+\tilde{C}-\varepsilon}-d_3\right)D,\ t>T_3,$$

which implies that $\limsup_{t\to\infty}D(t,q_3)=\infty$ since (18c) holds. A contradiction with (19c), and then (iii) holds.

If (19d) holds, then

$$\frac{\mathrm{d}C(t,q_4)}{\mathrm{d}t}\geq\left(e_1\min\left\{1,\frac{\bar{Q}-\varepsilon}{\theta_1}\right\}\frac{\sigma_1(\bar{A}-\varepsilon)}{a_1+\bar{A}-\varepsilon}-\frac{\sigma_3(\check{D}+\varepsilon)}{a_3}-d_2\right)C,\quad t>T_4,$$

which implies that $\limsup_{t\to\infty}C(t,q_4)=\infty$ since (18d) holds. A contradiction with (19d), and then (iv) holds. □

Theorem 10. *If $R_0>1$, $\max\{R_1^C,R_1^D\}>1$, $\hat{R}_2^D>1$, and $\hat{R}_3^C>1$, then model (5) is uniformly persistent with respect to $(\Delta,\partial\Delta)$, i.e., there exists a positive constant η such that*

$$\min\left\{\liminf_{t\to\infty}A(t,q_0),\liminf_{t\to\infty}C(t,q_0),\liminf_{t\to\infty}D(t,q_0),\liminf_{t\to\infty}Q(t,q_0)\right\}\geq\eta$$

for any $q_0=(A_0,C_0,D_0,Q_0)\in\Delta$. Furthermore, model (5) admits at least one coexistence equilibrium E^*.

Proof. Let $\omega(\bar{q}_0)$ be the omega limit set of the orbit $O^+(\bar{q}_0) := \{\Phi(t)\bar{q}_0 | t \geq 0\}$ for any $\bar{q}_0 \in \partial\Delta$. Obviously, $\Phi(t)\bar{q}_0 \in \partial\Delta$. We claim that $\omega(\bar{q}_0) \subset E_0 \cup E_1 \cup M_1 \cup M_2, \forall\, \bar{q}_0 \in \partial\Delta$. We prove it in the following four cases:

(i) If $A_0 = 0, C_0 = 0, D_0 = 0, Q_0 \neq 0$, then we have $A(t, \bar{q}_0) = 0$, $C(t, \bar{q}_0) = 0$, and $D(t, \bar{q}_0) = 0$ for all $t \geq 0$. From Theorem 5, $\lim\limits_{t\to\infty}(A(t, \bar{q}_0), C(t, \bar{q}_0), D(t, \bar{q}_0), Q(t, \bar{q}_0)) = (0, 0, 0, \hat{Q})$.

(ii) If $A_0 \neq 0, C_0 = 0, D_0 = 0, Q_0 \neq 0$, then one can obtain that $C(t, \bar{q}_0) = 0$ and $D(t, \bar{q}_0) = 0$ for all $t \geq 0$. From Theorem 6, $\lim_{t\to\infty}(A(t, \bar{q}_0), C(t, \bar{q}_0), D(t, \bar{q}_0), Q(t, \bar{q}_0)) = (A_1, 0, 0, Q_1)$.

(iii) If $A_0 \neq 0, C_0 \neq 0, D_0 = 0, Q_0 \neq 0$, then $D(t, \bar{q}_0) = 0$ for all $t \geq 0$. From Theorem 1, $(A(t, \bar{q}_0), C(t, \bar{q}_0), Q(t, \bar{q}_0))$ eventually enters Δ_2.

(iv) If $A_0 \neq 0, C_0 = 0, D_0 \neq 0, Q_0 \neq 0$, then $C(t, \bar{q}_0) = 0$ for all $t \geq 0$. From Theorem 1, $(A(t, \bar{q}_0), D(t, \bar{q}_0), Q(t, \bar{q}_0))$ eventually enters Δ_3.

This shows that the claim holds.

Based on the above discussion and Lemma 9, one can obtain the following conclusions: (1) $\{E_0, E_1, M_1, M_2\}$ is disjoint, compact, isolated invariant set in $\partial\Delta$; (2) E_0, E_1, M_1, and M_2 are isolated in Δ; (3) no subset of E_0, E_1, M_1, M_2 forms a cycle in $\partial\Delta$. By Lemma 9, E_i and M_j, $i = 0, 1, j = 1, 2$, are uniformly weak repellers for Δ. Therefore, $W^s(E_i) \cap \Delta = \emptyset$, $i = 0, 1$ and $W^s(M_j) \cap \Delta = \emptyset$, $j = 1, 2$, where $W^s(E_i)$ and $W^s(M_j)$ are the stable sets of E_i and M_j, respectively. By Theorem 1.3.1 in Zhao (2003), $\Phi(t)$ is uniformly persistence for $(\Delta, \partial\Delta)$. Furthermore, from Theorem 1.3.6 in Zhao (2003), $\Phi(t)$ admits a global attractor in Δ, and model (5) has at least one coexistence equilibrium $E^* \in \Delta$. □

Remark 2. *The condition of Theorem 10 is only a sufficient condition for the coexistence of algae, ciliate and* Daphnia. *They may also coexist if this condition does not hold. In addition, if* $\Delta_2 = \{(A_2, C_2, Q_2)\}$, *then* $\hat{R}_2^D$ *can be replaced by* R_2^D. *Similarly, if* $\Delta_3 = \{(A_3, D_3, Q_3)\}$, *then* $\hat{R}_3^C$ *can be replaced by* R_3^C.

5 Numerical simulations

In this section, we conduct some numerical simulations to illustrate the impact of environmental factors such as light intensity and nutrient concentration, as well as the phosphorus to carbon ratio of ciliate on the interactions among the three species: algae, ciliate, and *Daphnia*. The parameter values are presented in Table 2.

5.1 Effects of light intensity

Algae, through photosynthesis, transform solar energy into organic matter, thereby providing energy for aquatic food webs and playing a crucial role in sustaining the stability and biodiversity of aquatic ecosystems. Variations in light intensity can significantly impact algae quality, i.e., the cell quota Q, which can profoundly affect the dynamics of populations in food webs. Bifurcation diagrams provide a clear and visual means to investigate how system dynamics are influenced by specific parameters. Here we present the bifurcation diagram for model (5) concerning surface light intensity (I_{in}) in seawater under both P_i-deficient (Fig. 3) and P_i-sufficient conditions (Fig. 4).

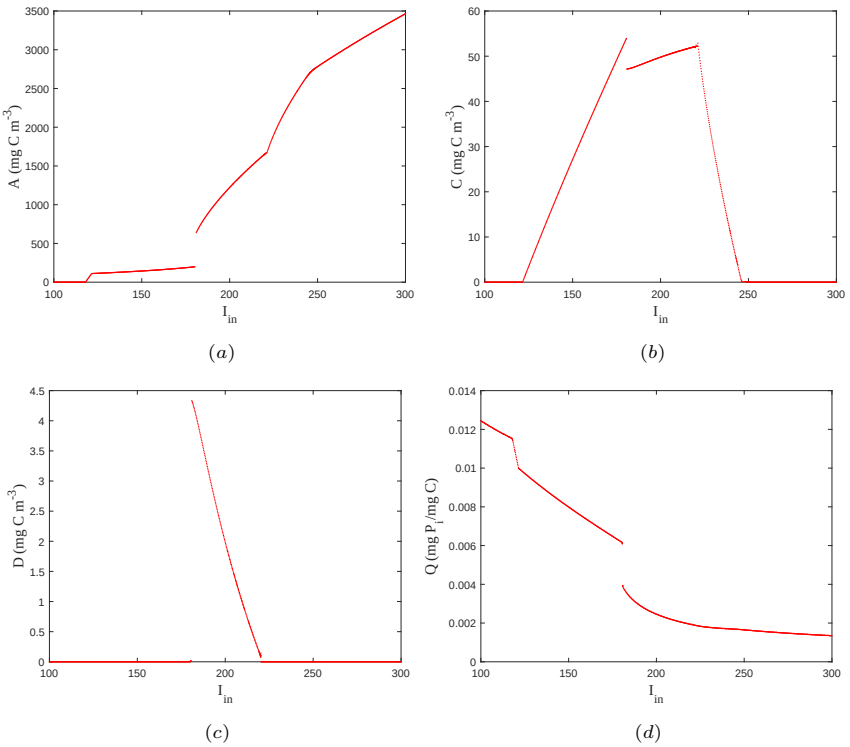

Fig. 3 Bifurcation diagram of model (5) with varying I_{in}. Here $P = 5$, $d_2 = 0.035$, and the resting parameter values are from in Table 2. Initial condition: (A(0), C(0), D(0), Q(0))=(50, 4, 2, 0.001).

Fig. 3 shows that when I_{in} is low ($0 < I_{in} < 118$), the photosynthetic activity of algae is limited, and the energy generated through photosynthesis falls short of sustaining algae growth, leading to the extinction of all three species. With a gradual increase in I_{in} ($118 < I_{in} < 121$), the photosynthesis of algae will be enhanced, resulting in a higher cell growth rate, thereby allowing the algae to survive. However, the light intensity at this stage cannot support the persistence of ciliate and *Daphnia*. As I_{in} further increases ($121 < I_{in} < 180$), algae can capture more energy, facilitating the survival of ciliate, but it is not adequate to sustain *Daphnia*. When I_{in} continues to increase ($180 < I_{in} < 221$), all species can coexist at a stable interior equilibrium E^*. Nevertheless, if the light intensity continues to increase, the quantity of algae will increase greatly but its quality will become extremely poor, which will lead to the extinction of ciliate and *Daphnia* due to lack of P_i. Specifically, if $221 < I_{in} < 247$, the quality of algae diminishes, and the intracellular P_i of algae and ciliate becomes insufficient to support the growth of *Daphnia*. In this case, *Daphnia* becomes extinct and the equilibrium E_2 is the attractor. If $I_{in} > 247$, the quality of algae further deteriorates, and the intracellular P_i of algae becomes inadequate to sustain ciliate, ultimately leading to ciliate extinction.

Fig. 4 shows the bifurcation results of model (5) with respect to I_{in} under P_i-sufficient condition. When light intensity is low ($I_{in} < 117.3$), none of the three species

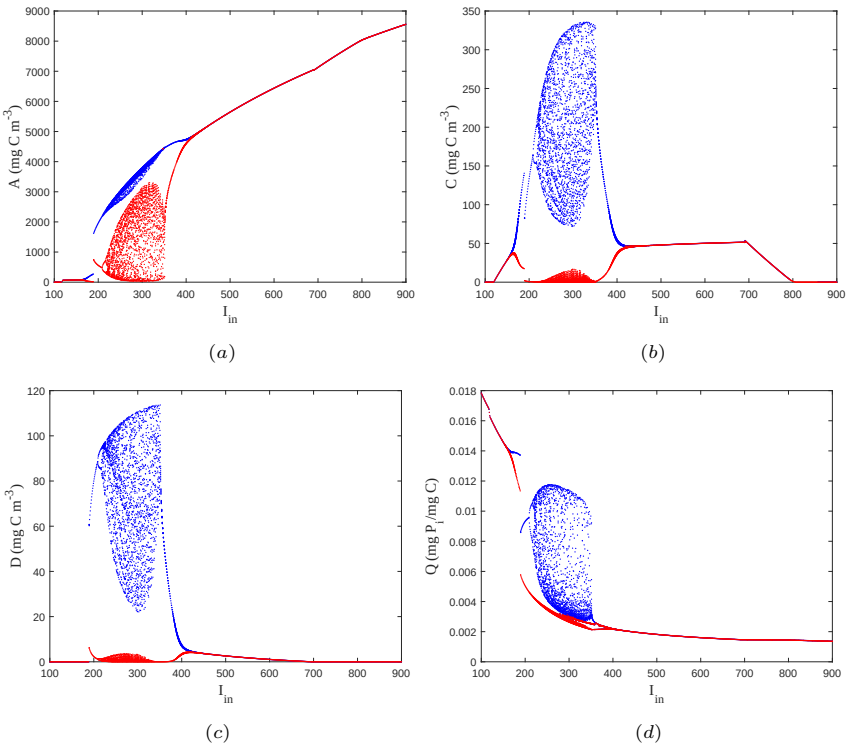

Fig. 4 Bifurcation diagram of model (5) with varying I_{in} (Blue dots: local maxima; Red dots: local minima). Here $P = 12$, $d = 0.035$ and the rest parameter values are from Table 2. The initial condition is the same as Fig. 3.

can persist. However, as I_{in} increases, algae, and ciliate can invade the system one after another. In the range of $117.3 < I_{in} < 119.4$, algae can survive, and the boundary equilibrium E_1 is the attractor. Subsequently, with I_{in} increases ($119.4 < I_{in} < 168$), ciliate can invade the aquatic ecosystem, allowing algae and ciliate to coexist at the stable boundary equilibrium E_2. As I_{in} increases through the threshold value of $I_{in} = 168$, a Hopf bifurcation appears and E_2 loses its stability. Therefore, a limit cycle emerges, and its amplitude grows with the increase of I_{in} within a reasonable interval ($168 < I_{in} < 189.6$). When I_{in} increases past the threshold value of 189.6, the dynamics of model (5) changes abruptly, the boundary limit cycle disappears, and an interior limit cycle will appear, i.e., all species coexist in the form of periodic oscillations. Then as I_{in} further increases, model (5) exhibits chaotic behavior through the period-doubling bifurcation. As I_{in} continues to increase, the irregular oscillation behavior of model (5) is replaced by periodic oscillation, ultimately stabilizing at an interior equilibrium E^*. When the light intensity is relatively high, the growth rate of algae increases and a large amount of low-quality algae are produced, causing ciliate and *Daphnia* to die out one after another due to the lack of P_i. This aligns with the findings of experiments, where higher algae abundance corresponds to lower ciliate and *Daphnia* abundance (Diehl et al, 2022). It is worth noting that, compared to the

case of P_i deficiency, under P_i sufficient conditions, the dynamics of model (5) become more intricate, and the three species may coexist in the form of periodic oscillations or irregular oscillations.

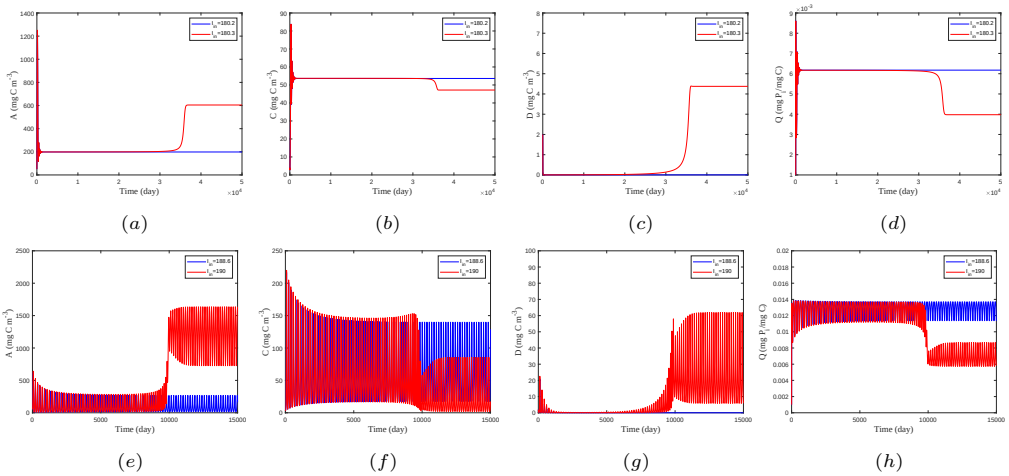

Fig. 5 Model (5) undergoes regime shifts with the change of I_{in}. (a)–(d) $P = 5$ and $d_2 = 0.035$; (e)–(h) $P = 12$ and $d_2 = 0.035$; The rest parameter values are from in Table 2. The initial condition is same as Fig. 3.

We also note that in Fig. 3, there is a discontinuous jump in the dynamics of model (5) from the boundary equilibrium E_2 to the positive equilibrium E^*. Specifically, when the light intensity I_{in} increases from 180.2 to 180.3, the biomass of *Daphnia* suddenly increases, and the biomass of algae and ciliate also experiences mutations (see the first row of Fig. 5). This phenomenon is widely recognized as the regime shift. A similar regime shift also occurs under P_i-sufficient (Fig. 4). With minor changes in I_{in}, the system dynamics can change from the boundary limit cycle to the interior limit cycle where three species coexist (see the second row of Fig. 5). Furthermore, Fig. 5 shows that model (5) displays long transient behavior, i.e. the duration of the transient can span tens or even hundreds of generations and then suddenly transitions to another regime (as shown in the red line in Fig. 5).

5.2 Effects of phosphate level

The concentration of P_i in the water directly affects the growth of algae, thereby affecting the interaction of species in the food web. In this subsection, we select P (total P_i) as the bifurcation parameter to simulate the impact of P_i level on the system dynamics. The bifurcation diagrams are shown in Fig. 6 ($\theta_1 = 0.0245$) and Fig. 7 ($\theta_1 = 0.03$).

Fig. 6 shows that when P_i concentration is deficient, algae will consume a large amount of intracellular P_i to maintain their growth, resulting in a decline in their quality (cell quota Q of algae is low). In this scenario, the energy enrichment paradox arises, ciliate and *Daphnia* cannot survive due to the poor food quality. As P increases,

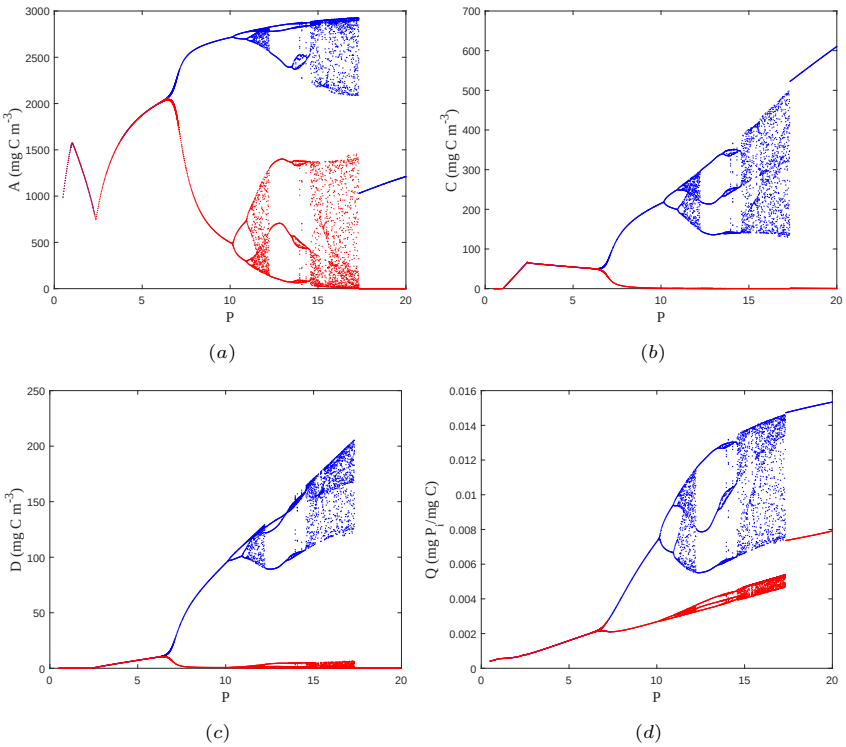

Fig. 6 Bifurcation diagram of model (5) with varying P (Blue dots: local maxima; Red dots: local minima). Here $\theta_1 = 0.0245$ and the rest parameter values are from in Table 2. The initial condition is same as Fig. 3.

algae can luxuriously absorb P_i from the environment and store it in their cells, and then the cell quota gradually increases. At this time, ciliate can rely on the intracellular P_i of algae to maintain growth, but the intracellular P_i of algae and ciliate cannot yet sustain the survival of *Daphnia* since it has higher P_i requirements. As P further increases, the intracellular P_i of algae becomes more abundant, allowing *Daphnia* to maintain their growth by preying on algae and ciliate. When $P = 6.93$, model (5) experiences a Hopf bifurcation. As P exceeds 6.93, the positive equilibrium E^* loses its stability, giving rise to a stable limit cycle where all species coexist in a regular oscillatory pattern. As P continues to increase, the system enters a phase of chaotic oscillations, with all species exhibiting irregular oscillations. However, with further increases in P, *Daphnia* becomes extinct, and algae and ciliate will coexist in a regular oscillation. This is because when P_i is sufficient, the competitive effect of ciliates and *Daphnia* on algae exceeds the predation effect of *Daphnia* on ciliate, and the principle of competitive exclusion is established. The phosphorus-to-carbon ratio of ciliate is closer to that of algae, so it has an advantage when competing with *Daphnia* for food, which eventually leads to the extinction of *Daphnia* due to starvation.

Fig. 7 depicts the impact of changes in P_i concentration in the environment on the model dynamics when the phosphorus to carbon ratio of ciliate is large. Comparing

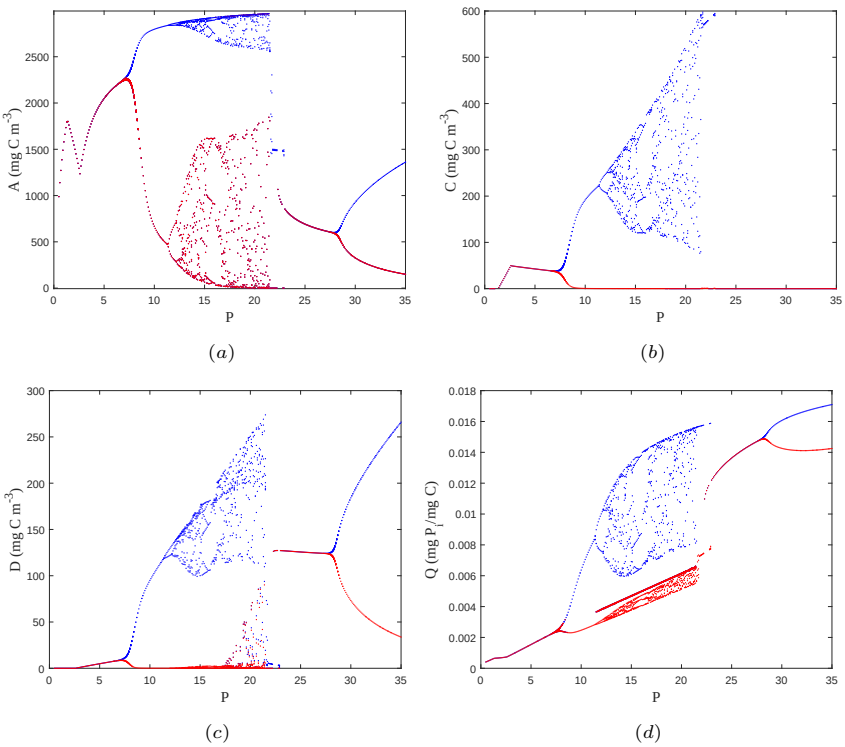

Fig. 7 Bifurcation diagram of model (5) with varying P (Blue dots: local maxima; Red dots: local minima). Here $\theta_1 = 0.03$ and the rest parameter values are from in Table 2. The initial condition is same as Fig. 3.

Figs. 6 and 7, we can see that as P increases, the dynamics of model (5) are similar to Fig. 6 at first, but when P is large enough, the system shows different dynamic behaviors. Specifically, when P_i concentration is high, ciliate is extinct, algae and *Daphnia* coexist first at a constant density and finally in a regular oscillation. This is because when the phosphorus-to-carbon ratio of the ciliate is close to that of *Daphnia*, the ciliate loses its competitive advantage under the predation pressure of *Daphnia*, which ultimately leads to the extinction of the ciliate. As can be seen from Figs. 6 and 7, the moderate P_i concentration is conducive to the coexistence of the three species, which is consistent with previous research results (Diehl, 2003; Loladze et al, 2004).

Note that model (5) will also undergo regime shifts as P changes small. When $\theta_1 = 0.0245$, the increase of P from 17.3 to 17.4 will destroy the chaotic coexistence state of all species, causing the dynamics of the system to tend to a boundary limit cycle (see the first row of Fig. 8). In addition, when $\theta_1 = 0.03$, the increase of P from 22.2 to 22.3 will lead to the transition of dynamics of model (5) from the interior limit cycle to boundary equilibrium E_3 (see the second row of Fig. 8).

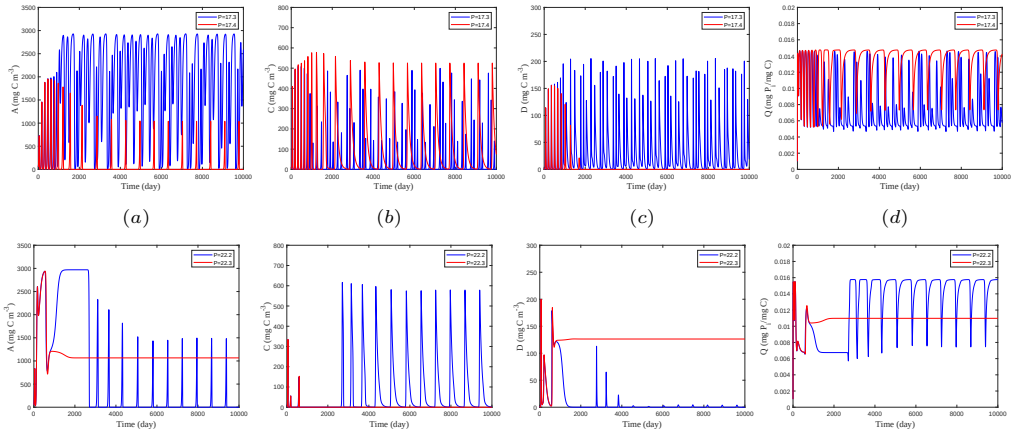

(a) (b) (c) (d)

(e) (f) (g) (h)

Fig. 8 Model (5) undergoes regime shifts with the change of P. (a)–(d) $\theta_1 = 0.0245$; (e)–(h) $\theta_1 = 0.03$; The rest parameter values are from in Table 2. The initial condition is same as Fig. 3.

5.3 Effects of the phosphorus to carbon ratio of ciliate

The IG prey (ciliate), which feeds on producers (algae) and is preyed by IG predator (*Daphnia*), plays an important role in the IGP system. Consequently, alterations in its phosphorus-to-carbon ratio can significantly influence the system dynamics. To investigate the impact of the quality of ciliate on system dynamics, we conduct a bifurcation analysis using θ_1 as the bifurcation parameter under the conditions of P_i-deficient ($P = 5$) and P_i-sufficient ($P = 15$), respectively.

It can be seen from Fig. 9 that when $\theta_1 \in (0.0003, 0.00766)$, algae and ciliate coexist in a form of periodic oscillation, while *Daphnia* becomes extinct. This is due to the phosphorus-to-carbon ratio of ciliate being close to that of algae, and the intracellular P_i in algae is sufficient to maintain the growth of ciliate. Despite the abundance of algae and ciliate, their P_i content is too low and constitutes poor-quality food for *Daphnia*, leading to the extinction of *Daphnia*. As θ_1 increases and surpasses the threshold value of 0.00766, the boundary limit cycle vanishes, and the boundary equilibrium E_2 becomes stable, which means that algae and ciliate can coexist with constant densities. With further increases in θ_1, the quality of ciliate improves, enabling sufficient intracellular P_i of algae and ciliate to sustain the growth of *Daphnia*. Thus, a scenario emerges where the three species coexist with constant densities for $\theta_1 \in (0.0177, 0.02546)$. Continuing the increase in θ_1, the demand for P_i by ciliate steadily increases, resulting in a gradual decline in the ciliate population due to P_i limitation. The reduction of ciliate alleviates the predation pressure on algae, leading to a rapid increase in algae quantity and a decrease in algae quality. Ultimately, both ciliate and *Daphnia* face extinction as they are unable to acquire sufficient P_i from algal cells. When $\theta_1 > 0.02546$, *Daphnia* becomes extinct, and then when $\theta_1 > 0.0293$, ciliate becomes extinct. The time series graph of model (5) under different θ_1 values in Fig. 10 reveals that as θ_1 increases, the dynamics of model (5) first stabilizes from the boundary limit cycle to the boundary equilibrium E_2, then transitions to positive equilibrium E^* where the three species

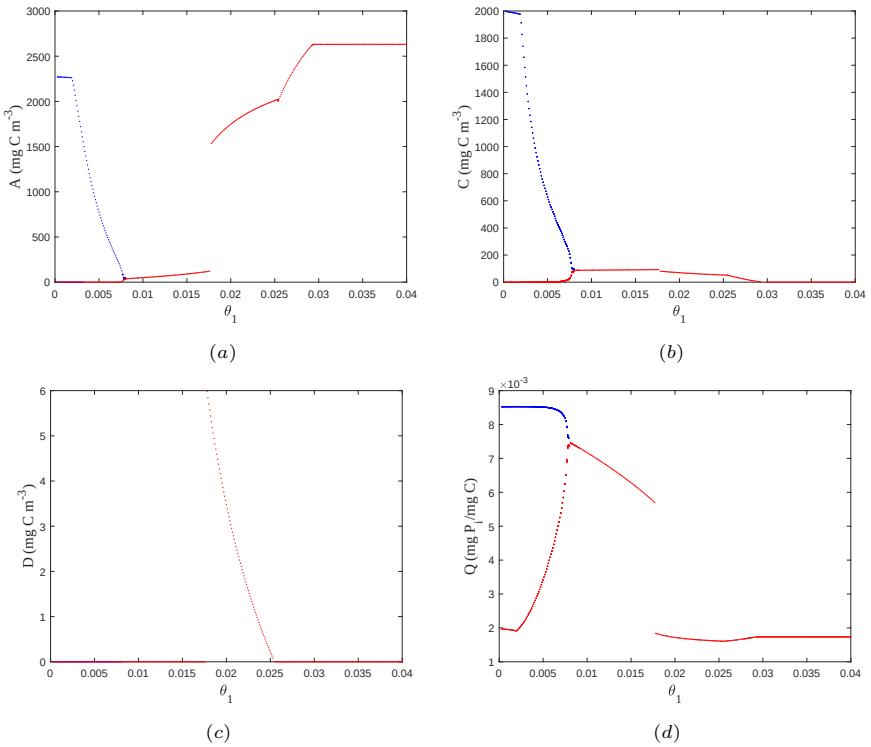

Fig. 9 Bifurcation diagram of model (5) with varying phosphorus to carbon ratio θ_1 of ciliate (Blue dots: local maxima; Red dots: local minima). Here $P = 5$, $d_2 = 0.03$ and the rest parameter values are from in Table 2. The initial condition is same as Fig. 3.

coexist with constant densities, and finally stabilizes at the only-algae exist equilibrium E_1. These results align with the bifurcation diagram of θ_1 (Fig. 9). Fig. 11 depicts the bifurcation results of model (5) with respect θ_1 under P_i-sufficient condition. It is evident that when P_i is sufficient, the impact of changes in θ_1 on system dynamics is similar to that observed under P_i-deficient. Notably, sufficient P_i augments the complexity of the dynamics of model (5). The system may exhibit chaotic behavior, where the three species coexist in the form of irregular oscillations. Furthermore, sufficient P_i expands the range of θ_1 that allows three species to coexist (Figs. 9 and 11). The above results show that the quality of ciliate has a significant impact on the dynamics of the IGP model. When the phosphorus-to-carbon ratio of ciliate is at an intermediate value, it is beneficial for the coexistence of species in the IGP food web. Conversely, a larger or smaller phosphorus-to-carbon ratio is not conducive to the coexistence of three species. Excessively large phosphorus-to-carbon ratio leads to the extinction of ciliate and *Daphnia* due to poor-quality algae, while smaller phosphorus-to-carbon ratio results in the extinction of *Daphnia* due to the poor quality of ciliate.

Obviously, a regime shift appears as θ_1 changes from 0.0177 to 0.01771 under P_i-deficient, resulting in a sudden increase in the biomass of algae and *Daphnia* (the first row of Fig. 12). This shift means a dynamics transition in model (5) from a

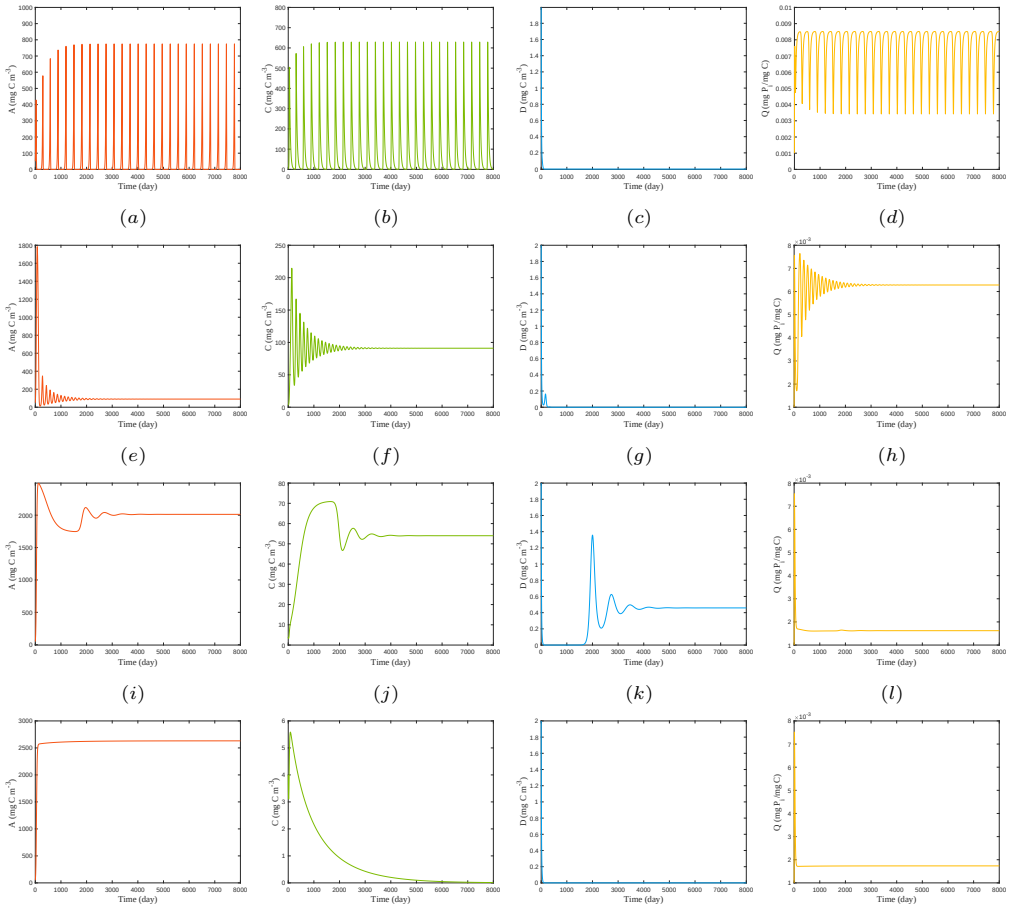

Fig. 10 Time series diagrams of model (5) for different values of phosphorus to carbon ratio θ_1 of ciliate. (a)–(d) $\theta_1 = 0.005$; (e)–(h) $\theta_1 = 0.015$; (i)–(l) $\theta_1 = 0.0245$; (m)–(p) $\theta_1 = 0.03$; Here $P = 5$, $d_2 = 0.03$, and the rest parameter values are from in Table 2. The initial condition is same as Fig. 3.

stable boundary equilibrium E_2 to a stable interior equilibrium E^* occurs. A similar regime shift occurs under P_i sufficient (second row of Fig. 12). Minor alterations in the phosphorus-to-carbon ratio of ciliate can trigger the transition of *Daphnia* from an extinct state to an irregular oscillation state. The dynamics of model (5) changes from a boundary limit cycle to a chaotic state where all species coexist. Note that the long transients are also observed in Fig. 12.

6 Discussion

In this study, we developed a novel stoichiometric IGP model by explicitly tracking the intracellular phosphate (P_i) of algae and free P_i in the environment. Furthermore, the effect of light intensity on algal growth was explicitly characterized in our model by

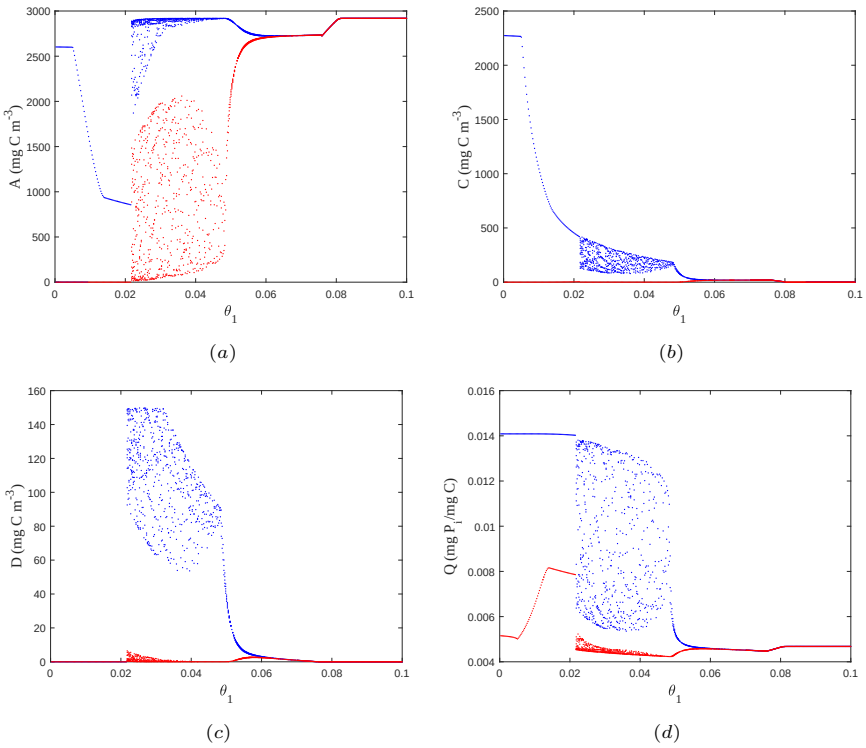

Fig. 11 Bifurcation diagram of model (5) with varying phosphorus to carbon ratio θ_1 of ciliate (Blue dots: local maxima; Red dots: local minima). Here $P = 15$, $d_2 = 0.03$, and the rest parameter values are from in Table 2. The initial condition is same as Fig. 3.

using the classical Droop and Monod equations, which help directly explore the impact of light intensity on system dynamics. This model was validated by the mesocosm experimental data of algae, ciliate, and *Daphnia* from Diehl et al (2022). The fitting results illustrated that our model can well capture the dynamics of the three species in the experiment. Theoretical and numerical analyses illustrated that the model exhibits complex dynamics, including chaos and multiple types of bifurcations, and undergoes long transients and regime shifts.

A comprehensive numerical analysis of the model was performed using the parameter values obtained from data fitting. The bifurcation analysis results of light intensity and total P_i revealed that they have an important influence on the growth and coexistence of the three species. Under extremely low light intensity, the photosynthesis of algae is too low to maintain species survival, leading to the extinction of all species (Fig. 3). With increasing light intensity, algae, ciliate, and *Daphnia* can successfully invade the system one after another. At moderate light levels, the three species can coexist with constant densities, periodic oscillations, or irregular oscillations. In the high-light environment, the system will be limited by P_i, producing a large amount of low-quality algae, leading to the extinction of ciliate and *Daphnia* due to P_i deficiency (Fig. 3). Notably, *Daphnia* has a higher demand for P_i than ciliate ($\theta_1 < \theta_2$), so

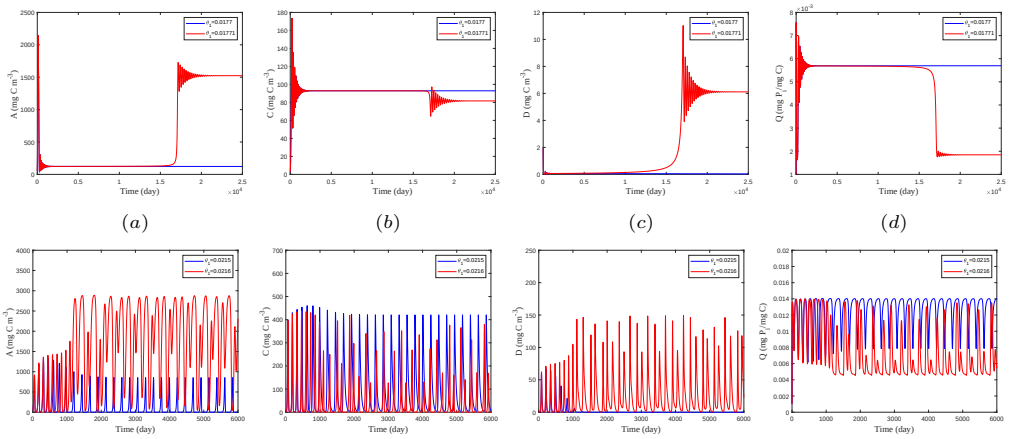

Fig. 12 Model (5) undergoes regime shifts with the change of phosphorus to carbon ratio θ_1 of ciliate. (a)–(d) $P = 5$ and $d_2 = 0.03$; (e)–(h) $P = 15$ and $d_2 = 0.03$; The rest parameter values are from in Table 2. The initial condition is same as Fig. 3.

Daphnia usually dies out before ciliate due to P_i deficiency (Figs. 3 and 4). Furthermore, our numerical results indicated that under P_i-insufficient conditions, no matter how the light intensity changes, it will not cause the coexistence of populations in the form of periodic or irregular oscillations (Fig. 3). This showed that the lower P_i concentration in the environment is not enough to maintain the complex dynamics of the system. Conversely, in a high-P_i environment, the three species are more prone to exhibiting complex coexistence patterns, such as periodic oscillations and irregular oscillations (Fig. 4).

At a constant light intensity, an increase in the available P_i concentration within the system leads to progressively intricate dynamics, including the emergence of a limit cycle, period-doubling bifurcation, and even chaotic phenomena. Similar to the results observed in light intensity simulations, the coexistence of the three species occurs at an intermediate level of available P_i, with both lower and higher concentrations leading to the extinction of ciliate or *Daphnia* (Figs. 6 and 7). Specifically, at low P_i concentration, ciliate and *Daphnia* will become extinct by eating poor-quality algae, which is known as the energy enrichment paradox. If the concentration of P_i is high, the quality of the algae will be improved, which will intensify the competition between ciliate and *Daphnia* for algae, leading to the competitive exclusion (Diehl, 2003; Loladze et al, 2004). When the phosphorus to carbon ratio of ciliate is close to that of algae, ciliate has a competitive advantage, and with the increase of concentration of P_i, *Daphnia* eventually becomes extinct (Fig. 6). If the phosphorus to carbon ratio of ciliate is close to that of *Daphnia*, then *Daphnia* will gain a competitive advantage, eventually leading to the extinction of ciliate (Fig. 7). This is consistent with the existing findings that stable coexistence of consumers and omnivores is not possible when the quality of shared prey is high (Diehl, 2003; Loladze et al, 2004; Elser et al, 2012). Furthermore, our simulations revealed that small adjustments in light intensity and P_i concentration near critical values result in abrupt shifts in the system (Figs. 3

and 12). The regime shift may lead to the extinction of the population and harm the biodiversity of the ecosystem. This phenomenon is common in ecosystems, for example, during the initial stages of harmful algal blooms, where changes in light intensity or P_i concentration can trigger rapid algae proliferation. Similarly, during the later stages of a harmful algal bloom, alterations in the environment may lead to a sudden decline in algae density.

In our model, as with many stoichiometric models, we assume a constant phosphorus to carbon ratio for ciliate and *Daphnia*. This hypothesis is based on the understanding that while predator phosphorus-to-carbon ratio may vary, the extent of this variation is relatively small compared to changes in producers. Nonetheless, recent research challenged this assumption of strict homeostasis, demonstrating that phosphorus to carbon ratio in consumers can exhibit considerable flexibility (Prater et al, 2017; Teurlincx et al, 2017). To explore the reliability and availability of strict hypothesis assumptions, Wang et al (2012) established one-nutrient and two-nutrient stoichiometry models by tracking the phosphorus-to-carbon ratio of herbivores. They defined a hard dynamic threshold for herbivore stoichiometric variability, and when herbivore stoichiometric variability is smaller than this threshold, the strict homeostasis assumption can be applied. Building on this work, Wang et al (2018) extended the model to include light/energy dynamics, establishing a weak dynamic threshold. Under the weak dynamic threshold definition, the strict homeostasis assumption is more likely to hold, which further supports the conclusion that strict herbivore homeostasis can be assumed for most herbivores.

To investigate the influence of the phosphorus-to-carbon ratio of ciliate on the dynamics of the IGP model, a bifurcation analysis of θ_1 was performed. The results illustrated that variations in θ_1 significantly impact system dynamics. A low phosphorus-to-carbon ratio of ciliate will lead to the extinction of *Daphnia*, whereas a high phosphorus to carbon ratio of ciliate will cause algae to lose control and produce a large amount of low-quality algae, causing ciliate and *Daphnia* to become extinct due to P_i deficiency. Our simulation results indicated that if the ciliate maintains an appropriate phosphorus-to-carbon ratio, the coexistence of the three species is feasible, and the energy enrichment paradox can be avoided (Figs. 9 and 12). Because ciliate has a higher phosphorus-to-carbon ratio than algae, they can trophically upgrade poor quality algae, which can alleviate the degree of the stoichiometric mismatch between algae and *Daphnia*, mitigating *Daphnia* extinction risk (Golz et al, 2015; Declerck and de Senerpont Domis, 2023).

Therefore, it is necessary to consider the variations in consumer phosphorus to carbon ratio in future studies, which could help deepen the understanding of species coexistence and ecological diversity. In addition, the coexistence mechanism of the three species is intricate and can appear as positive equilibrium, regular oscillations, or irregular oscillations. In the theoretical analysis, we only proved the existence of positive equilibrium. The remaining two coexistence forms are given in numerical simulations. Rigorous proof of these two coexistence mechanisms is a challenging open problem.

Acknowledgments

S. Yuan and S. Gao are partially supported by the National Natural Science Foundation of China (No.11671260; 12071293) and the Natural Science Foundation of Shanghai Municipality (No. 23ZR1445100). H. Wang is partially funded by the Natural Sciences and Engineering Research Council of Canada (Individual Discovery Grant RGPIN-2020-03911 and Discovery Accelerator Supplement Award RGPAS-2020-00090). We are very grateful to both the editor and the reviewers for their valuable comments and suggestions, which have greatly improved the quality and presentation of our paper.

Data Availability

All data generated or analyzed during this study is included in this article.

Declarations

Conflict of interest The authors declare that they have no conflict of interest.

Appendix

To analyze the stability of the boundary equilibria, we first compute the Jacobian matrix of model (5), which is shown below

$$J = \begin{pmatrix} F + AF_A & AF_C & AF_D & AF_Q \\ CG_A & G + CG_C & CG_D & CG_Q \\ DH_A & DH_C & H & DH_Q \\ W_A & W_C & W_D & W_Q \end{pmatrix},$$

where

$$\begin{aligned}
F_A =& \mu_{\max}\left(1 - \frac{Q_m}{Q}\right)\bar{I}'(A) + \frac{\sigma_1 C}{(a_1 + A)^2} + \frac{\sigma_2 D}{(a_2 + A)^2},\\
F_C =& -\frac{\sigma_1}{a_1 + A},\ F_D = -\frac{\sigma_2}{a_2 + A},\ F_Q = \frac{\mu_{\max}\bar{I}(A)Q_m}{Q^2},\\
G_A =& \begin{cases} \frac{e_1\sigma_1 a_1}{(a_1+A)^2}, & Q > \theta_1, \\ \frac{Qe_1\sigma_1 a_1}{\theta_1(a_1+A)^2}, & Q < \theta_1, \end{cases} G_Q = \begin{cases} 0, & Q > \theta_1, \\ \frac{e_1\sigma_1 A}{\theta_1(a_1+A)}, & Q < \theta_1, \end{cases} G_C = \frac{\sigma_3 D}{(a_3 + C)^2},\ G_D = -\frac{\sigma_3}{a_3 + C},\\
H_A =& \begin{cases} \frac{e_2\sigma_2 a_2}{(a_2+A)^2}, & Q > \theta_2, \\ \frac{Qe_2\sigma_2 a_2}{\theta_2(a_2+A)^2}, & Q < \theta_2, \end{cases} H_C = \begin{cases} \frac{e_3\sigma_3 a_3}{(a_3+C)^2}, & \theta_1 > \theta_2, \\ \frac{\theta_1 e_3\sigma_3 a_3}{\theta_2(a_3+C)^2}, & \theta_1 < \theta_2, \end{cases} H_Q = \begin{cases} 0, & Q > \theta_2, \\ \frac{e_2\sigma_2 A}{\theta_2(a_2+A)}, & Q < \theta_2, \end{cases}
\end{aligned}$$

$$
\begin{aligned}
W_A =& -\frac{\gamma K_p Q(Q_M - Q)}{(P - AQ - \theta_1 C - \theta_2 D + K_p)^2 (Q_M - Q_m)} - \mu_{\max}\left(1 - \frac{Q_m}{Q}\right)\bar{I}'(A)Q,\\
W_C =& -\frac{\gamma \theta_1 K_p (Q_M - Q)}{(P - AQ - \theta_1 C - \theta_2 D + K_p)^2 (Q_M - Q_m)},\\
W_D =& -\frac{\gamma \theta_2 K_p (Q_M - Q)}{(P - AQ - \theta_1 C - \theta_2 D + K_p)^2 (Q_M - Q_m)},\\
W_Q =& \frac{-\gamma A K_p (Q_M - Q) - \gamma (P - AQ - \theta_1 C - \theta_2 D)}{(P - AQ - \theta_1 C - \theta_2 D + K_p)^2 (Q_M - Q_m)} - \mu_{\max}\bar{I}(A).
\end{aligned}
$$

A Proof of Theorem 5

The Jacobian matrix at E_0 is

$$
J(E_0) = \begin{pmatrix} a_{11} & 0 & 0 & 0 \\ 0 & -d_2 & 0 & 0 \\ 0 & 0 & -d_3 & 0 \\ a_{41} & a_{42} & a_{43} & a_{44} \end{pmatrix}.
$$

Obviously, a_{11}, $-d_2$, $-d_3$, and a_{44} are the four eigenvalues of the characteristic equation of $J(E_0)$, where $a_{11} = \mu_{\max}\left(1 - \frac{Q_m}{\hat{Q}}\bar{I}(0)\right) - d_1$ and $a_{44} = -\frac{\gamma P}{(P+K_p)(Q_M - Q_m)} - \mu_{\max}\bar{I}(0) < 0$. If $R_0 < 1$, then $a_{11} < 0$, and hence all eigenvalues of the characteristic equation of $J(E_0)$ have negative real parts, which indicates that E_0 is locally asymptotically stable. If $R_0 > 1$, then $a_{11} > 0$, which means that E_0 is unstable.

Now we prove E_0 is a global attractor when $\hat{R}_0 < 1$. By the first equation of model (5), we have

$$
\frac{\mathrm{d}A}{\mathrm{d}t} = \mu_{\max}\left(1 - \frac{Q_m}{Q}\right)\bar{I}(A)A - \frac{\sigma_1 AC}{a_1 + A} - \frac{\sigma_2 AD}{a_2 + A} - d_1 A < \left(\mu_{\max}\left(1 - \frac{Q_m}{Q_M}\right)\bar{I}(0) - d_1\right)A,
$$

which illustrates that $\limsup_{t\to\infty} A(t) = 0$ if $\hat{R}_0 < 1$. Then the second equation of model (5) becomes

$$
\frac{\mathrm{d}C}{\mathrm{d}t} = -\frac{\sigma_3 CD}{a_3 + C} - d_2 C,
$$

which implies that $\limsup_{t\to\infty} C(t) = 0$. Similarly, we can obtain that $\limsup_{t\to\infty} D(t) = 0$. The last equation of model (5) can be rewritten as

$$
\frac{\mathrm{d}Q}{\mathrm{d}t} = \frac{\gamma P(Q_M - Q)}{(P + K_p)(Q_M - Q_m)} + \mu_{\max}\bar{I}(0)(Q_m - Q).
$$

This means that $\limsup_{t\to\infty} Q(t) = \hat{Q}$. Therefore, in summary, E_0 is a globally attractor. Note that $R_0 < \hat{R}_0$, then $\hat{R}_0 < 1$ implies that E_0 is locally asymptotically stable. Thus E_0 is globally asymptotically stable if $\hat{R}_0 < 1$. □

B Proof of Theorem 6

The Jacobian matrix at E_1 is

$$J(E_1) = \begin{pmatrix} a_{11} & a_{12} & a_{13} & a_{14} \\ 0 & a_{22} & 0 & 0 \\ 0 & 0 & a_{33} & 0 \\ a_{41} & a_{42} & a_{43} & a_{44} \end{pmatrix},$$

where

$$\begin{aligned}
a_{11} =& \mu_{\max}\left(1-\frac{Q_m}{Q_1}\right)\bar{I}'(A_1)A_1 < 0,\ a_{22} = e_1 \min\left\{1, \frac{Q_1}{\theta_1}\right\}\frac{\sigma_1 A_1}{a_1+A_1} - d_2,\\
a_{33} =& e_2 \min\left\{1, \frac{Q_1}{\theta_2}\right\}\frac{\sigma_2 A_1}{a_2+A_1} - d_3,\ a_{14} = \frac{\mu_{\max} Q_m A_1 \bar{I}(A_1)}{Q_1^2} > 0,\\
a_{41} =& -\frac{\gamma K_p Q_1 (Q_M - Q_1)}{(P - A_1Q_1 + K_p)^2 (Q_M - Q_m)} - \mu_{\max}\left(1-\frac{Q_m}{Q_1}\right)\bar{I}'(A_1)Q_1,\\
a_{44} =& -\frac{\gamma K_p A_1 (Q_M - Q_1)}{(P - A_1Q_1 + K_p)^2 (Q_M - Q_m)} - \frac{\gamma(P - A_1Q_1)}{(P - A_1Q_1 + K_p)(Q_M - Q_m)} - \mu_{\max}\bar{I}(A_1) < 0.
\end{aligned}$$

Note that a_{22} and a_{33} are two eigenvalues of characteristic equation of $J(E_1)$, and the rest two eigenvalues satisfy the equation

$$\lambda^2 - (a_{11}+a_{44})\lambda + a_{11}a_{44} - a_{14}a_{41} = 0. \tag{20}$$

By simple calculations, one can check that $a_{11}a_{44} - a_{14}a_{41} > 0$. Note that $a_{11}+a_{44} < 0$, then all roots of equation (20) have negative real parts. If $\max\left\{R_1^C, R_1^D\right\} < 1$, then $a_{22} < 0$ and $a_{33} < 0$, and hence all eigenvalues of characteristic equation of $J(E_1)$ have negative real parts, which means that E_1 is locally asymptotically stable. Conversely, if $\max\left\{R_1^C, R_1^D\right\} > 1$, E_1 is unstable.

Now we prove that E_1 is globally asymptotically stable. The second equation of model (5) can be expressed as

$$\frac{\mathrm{d}C}{\mathrm{d}t} = e_1 \min\left\{1, \frac{Q}{\theta_1}\right\}\frac{\sigma_1 AC}{a_1+A} - \frac{\sigma_3 CD}{a_3+C} - d_2 C < \left(e_1\sigma_1 \min\left\{1, \frac{Q_M}{\theta_1}\right\} - d_2\right)C,$$

which implies that $\limsup_{t\to\infty} C(t) = 0$ if $\hat{R}_1^C < 1$. Then the third equation of model (5) can be rewritten as

$$\frac{\mathrm{d}D}{\mathrm{d}t} = e_2 \min\left\{1, \frac{Q}{\theta_2}\right\}\frac{\sigma_2 AD}{a_2+A} - d_3 D < \left(e_2\sigma_2 \min\left\{1, \frac{Q_M}{\theta_2}\right\} - d_3\right)D,$$

which means that $\limsup_{t\to\infty} D(t) = 0$ if $\hat{R}_1^D < 1$. In autonomous system (5), both $C(t)$ and $D(t)$ converge to 0. Therefore, we can use the following limit system to

consider the behavior of the solution of system (5) when $D = 0$ and $C = 0$,

$$\begin{aligned}\frac{\mathrm{d}A}{\mathrm{d}t} =&\mu_{\max}\left(1-\frac{Q_m}{Q}\right)\bar{I}(A)A - d_1 A,\\ \frac{\mathrm{d}Q}{\mathrm{d}t} =&\frac{\gamma(P-AQ)(Q_M-Q)}{(P-AQ+K_p)(Q_M-Q_m)} - \mu_{\max}\left(1-\frac{Q_m}{Q}\right)\bar{I}(A)Q.\end{aligned} \tag{21}$$

Define $\Delta_1 = \{(A,Q)|0 < A,\ Q_m < Q < Q_M,\ AQ < P\}$. From Theorem 1, Δ_1 is the positive invariant set of system (21). System (21) is the limit system of asymptotically autonomous system (5) under the constraint $\max\{R_1^C, R_1^D\} < 1$. The results of Markus (1956) and Thieme (1992) allow us to compare the solutions of autonomous system with those of asymptotically autonomous limit systems. Obviously, model (21) has two equilibria $\tilde{E}_0 = (0, \hat{Q})$ and $\tilde{E}_1 = (A_1, Q_1)$ when $R_0 > 1$. It is easy to know from Theorems 5 and 6 $\tilde{E}_0$ is unstable and $\tilde{E}_1$ is locally asymptotically stable if $R_0 > 1$.

Note that

$$\frac{\partial A'}{\partial A}+\frac{\partial Q'}{\partial Q} = \mu_{\max}\left(1-\frac{Q_m}{Q}\right)\bar{I}'(A)A - d_1 - \frac{\gamma A K_p(Q_M-Q)+\gamma(P-AQ)}{(P-AQ+K_p)^2(Q_M-Q_m)} - \frac{\mu_{\max}Q_m\bar{I}(A)}{Q} < 0.$$

Therefore, model (21) has no periodic orbit in Δ_1 by using the Dulac-Bendixson theorem. Note also that Δ_1 is simply connected and a positive invariant set of system (21). Therefore, according to Poincaré-Bendixson theorem, all solutions of system (21) starting in Δ_1 will converge to $\tilde{E}_1$ when $R_0 > 1$. Thus, $\tilde{E}_1$ is globally asymptotically stable. The omega limit set of the forward bounded solution of the autonomous system (5) consists of the equilibrium of its limit autonomous system (21) (Thieme, 1992). Hence, the omega limit set of system (5) is $\{E_1\}$ when $R_0 > 1$ and $\max\{\hat{R}_1^C, \hat{R}_1^D\} < 1$. The algae-only equilibrium E_1 is globally asymptotically stable if $R_0 > 1$ and $\max\{\hat{R}_1^C, \hat{R}_1^D\} < 1$. □

C Proof of Theorem 7

The Jacobian matrix at E_2 is

$$J(E_2) = \begin{pmatrix} a_{11} & a_{12} & a_{13} & a_{14} \\ a_{21} & 0 & a_{23} & a_{24} \\ 0 & 0 & a_{33} & 0 \\ a_{41} & a_{42} & a_{43} & a_{44} \end{pmatrix},$$

where

$$
\begin{aligned}
a_{11} =& \mu_{\max}\left(1-\frac{Q_m}{Q_2}\right)\bar{I}'(A_2)A_2+\frac{\sigma_1 C_2 A_2}{(a_1+A_2)^2},\ a_{12}=-\frac{\sigma_1 A_2}{a_1+A_2}<0,\\
a_{21} =& \begin{cases} \frac{e_1\sigma_1 a_1 C_2}{(a_1+A_2)^2}>0, & Q_2>\theta_1,\\ \frac{e_1\sigma_1 a_1 C_2 Q_2}{\theta_1(a_1+A_2)^2}>0, & Q_2<\theta_1, \end{cases}
a_{24} = \begin{cases} 0, & Q_2>\theta_1,\\ \frac{e_1\sigma_1 A_2 C_2}{\theta_1(a_1+A_2)}>0, & Q_2<\theta_1, \end{cases}\\
a_{33} =& e_2\min\left\{1,\frac{Q_2}{\theta_2}\right\}\frac{\sigma_2 A_2}{a_2+A_2}+e_3\min\{1,\frac{\theta_1}{\theta_2}\}\frac{\sigma_3 C_2}{a_3+C_2}-d_3,\\
a_{41} =& -\frac{\gamma K_p Q_2(Q_M-Q_2)}{(P-AQ_2-\theta_1 C_2+K_p)^2(Q_M-Q_m)}-\mu_{\max}\left(1-\frac{Q_m}{Q_2}\right)\bar{I}'(A_2)Q_2,\\
a_{42} =& \frac{-\gamma\theta_1 K_p(Q_M-Q_2)}{(P-A_2Q_2-\theta_1 C_2+K_p)^2(Q_M-Q_m)}<0,\ a_{14}=\frac{\mu_{\max}\bar{I}(A_2)Q_m A_2}{Q_2^2}>0,\\
a_{44} =& \frac{-\gamma A_2 K_p(Q_M-Q_2)-\gamma(P-A_2Q_2-\theta_1 C_2)}{(P-A_2Q_2-\theta_1 C_2+K_p)^2(Q_M-Q_m)}-\mu_{\max}\bar{I}(A_2)<0.
\end{aligned}
$$

Note that a_{33} is one eigenvalue of characteristic equation of $J(E_2)$, and the rest three eigenvalues satisfy the equation

$$\lambda^3+b_1\lambda^2+b_2\lambda+b_3=0, \tag{22}$$

where $b_1=-(a_{11}+a_{44})$, $b_2=a_{11}a_{44}-a_{14}a_{41}-a_{24}a_{42}-a_{12}a_{21}$, $b_3=-a_{12}a_{24}a_{41}-a_{21}a_{14}a_{42}+a_{11}a_{24}a_{42}+a_{12}a_{21}a_{44}$. If $R_2^D>1$, then $a_{33}>0$, which means that E_2 is unstable. When $R_2^D<1$, we prove the stability of E_2 in the following two cases.

Case 1. Suppose that $Q_2>\theta_1$, then $a_{21}=\frac{e_1\sigma_1 a_1}{(a_1+A_2)^2}>0$ and $a_{24}=0$. Hence $b_2=a_{11}a_{44}-a_{14}a_{41}-a_{12}a_{21}$ and $b_3=-a_{21}a_{14}a_{42}+a_{12}a_{21}a_{44}>0$. If

$$d_1>d_1^*=\mu_{\max}\left(1-\frac{Q_m}{Q_2}\right)\left(\bar{I}'(A_2)\Big(1-\frac{Q_m}{Q_2}\Big)(a_1+A_2)+\bar{I}(A_2)\right),$$

then $a_{11}=\mu_{\max}\left(1-\frac{Q_m}{Q_2}\right)\left(\bar{I}'(A_2)A_2+\frac{A_2}{a_1+A_2}\bar{I}(A_2)\right)-\frac{d_1A_2}{a_1+A_2}<0$. By simple calculations, one can obtain that $b_1>0$ and $b_1b_2-b_3>0$ if $d_1>d_1^*$. Therefore, according to the Routh-Hurwitz criterion, all roots of equation (22) have negative real parts.

Case 2. Assume that $Q_2<\theta_1$, then $a_{21}=\frac{e_1\sigma_1 a_1 C_2 Q_2}{\theta_1(a_1+A_2)^2}>0$ and $a_{24}=\frac{e_1\sigma_1 A_2 C_2}{\theta_1(a_1+A_2)}>0$. By simple calculations, we can obtain that $b_1>0$, $b_3>0$ and $b_1b_2-b_3>0$, if

$$d_1>d_1^{**}=\mu_{\max}\left(1-\frac{Q_m}{Q_2}\right)\left(\bar{I}'(A_2)\Big(a_1+A_2-\frac{e_1Q_2\sigma_1}{\theta_1}\Big)+\bar{I}(A_2)\right)$$

and $a_{21}a_{44}<a_{41}a_{24}$ hold. Hence all roots of equation (22) have negative real parts.

Note that if $R_2^D<1$, then $a_{33}<0$. Therefore, all eigenvalues of $J(E_2)$ have negative real parts if case (1) or case (2) hold, which means that E_2 is locally asymptotically stable. □

References

Arim M, Marquet PA (2004) Intraguild predation: a widespread interaction related to species biology. Ecol Lett 7(7):557–564

Arrigo KR (2005) Marine microorganisms and global nutrient cycles. Nature 437(7057):349–355

Chen M, Fan M, Liu R, et al (2015) The dynamics of temperature and light on the growth of phytoplankton. J Theor Biol 385:8–19

Chen M, Fan M, Kuang Y (2017) Global dynamics in a stoichiometric food chain model with two limiting nutrients. Math Biosci 289:9–19

Chen M, Gong ML, Zhang J, et al (2023) Comparison of dynamic behavior between continuous-and discrete-time models of intraguild predation. Math Biosci Eng 20(7):12750–12771

De Senerpont Domis LN, Van de Waal DB, Helmsing NR, et al (2014) Community stoichiometry in a changing world: combined effects of warming and eutrophication on phytoplankton dynamics. Ecology 95(6):1485–1495

Declerck SAJ, de Senerpont Domis LN (2023) Contribution of freshwater metazooplankton to aquatic ecosystem services: an overview. Hydrobiologia 850(12-13):2795–2810

Diehl S (2003) The evolution and maintenance of omnivory: dynamic constraints and the role of food quality. Ecology 84(10):2557–2567

Diehl S, Berger S, Wöhrl R (2005) Flexible nutrient stoichiometry mediates environmental influences on phytoplankton and its resources. Ecology 86(11):2931–2945

Diehl S, Berger SA, Uszko W, et al (2022) Stoichiometric mismatch causes a warming-induced regime shift in experimental plankton communities. Ecology (5):103

Elser JJ, Loladze I, Peace AL, et al (2012) Lotka re-loaded: Modeling trophic interactions under stoichiometric constraints. Ecol Model 245:3–11

Gao SF, Shen AL, Jiang J, et al (2022) Kinetics of phosphate uptake in the dinoflagellate *Karenia mikimotoi* in response to phosphate stress and temperature. Ecol Model 468:109909

Golz AL, Burian A, Winder M (2015) Stoichiometric regulation in micro-and mesozooplankton. J Plankton Res 37(2):293–305

Guedes VC, Palma GM, Horta ACL (2023) An evaluation of light wavelengths, intensity and control for the production of microalgae in photobioreactors: a review. Braz J Chem Eng pp 1–14

774 Guest JS, Van Loosdrecht MCM, Skerlos SJ, et al (2013) Lumped pathway metabolic
775 model of organic carbon accumulation and mobilization by the alga chlamydomonas
776 reinhardtii. Environ Sci Technol 47(7):3258–3267

777 Hall RJ (2011) Intraguild predation in the presence of a shared natural enemy. Ecology
778 92(2):352–361

779 Holling CS (1965) The functional response of predators to prey density and its role in
780 mimicry and population regulation. Mem Ent Canada 97(45):3–60

781 Holt RD, Polis GA (1997) A theoretical framework for intraguild predation. Am Nat
782 149(4):745–764

783 Hsu SB, Ruan SG, Yang TH (2015) Analysis of three species lotka–volterra food web
784 models with omnivory. J Math Anal Appl 426(2):659–687

785 Huisman J, Weissing FJ (1994) Light-limited growth and competition for light in
786 well-mixed aquatic environments: an elementary model. Ecology 75(2):507–520

787 Ji JP, Lin GH, Wang L, et al (2022) Spatiotemporal dynamics induced by intraguild
788 predator diffusion in an intraguild predation model. J Math Biol 85(1):1

789 Ji JP, Milne R, Wang H (2023) Stoichiometry and environmental change drive dynami-
790 cal complexity and unpredictable switches in an intraguild predation model. J Math
791 Biol 86(2):31

792 Kang Y, Wedekin L (2013) Dynamics of a intraguild predation model with generalist
793 or specialist predator. J Math Biol 67:1227–1259

794 Lee E, Jalalizadeh M, Zhang Q (2015) Growth kinetic models for microalgae
795 cultivation: a review. Algal Res 12:497–512

796 Li X, Wang H, Kuang Y (2011) Global analysis of a stoichiometric producer–grazer
797 model with holling type functional responses. J Math Biol 63(5):901–932

798 Liu L, Zhang H, Liu X, et al (2023) The comprehensive effect of natural food quality
799 and quantity on growth rate of herbivore consumers. Ecol Indic 156:111129

800 Loladze I, Kuang Y, Elser JJ (2000) Stoichiometry in producer-grazer systems: Linking
801 energy flow with element cycling. B Math Biol 62(6):1137–1162

802 Loladze I, Kuang Y, Elser JJ, et al (2004) Competition and stoichiometry: coexistence
803 of two predators on one prey. Theor Popul Biol 65(1):1–15

804 Lonsinger RC, Gese EM, Bailey LL, et al (2017) The roles of habitat and intraguild
805 predation by coyotes on the spatial dynamics of kit foxes. Ecosphere 8(3):e01749

López Muñoz I, Bernard O (2021) Modeling the influence of temperature, light intensity and oxygen concentration on microalgal growth rate. Processes 9(3):496

Markus L (1956) Asymptotically autonomous differential systems. In: Contributions to the theory of nonlinear oscillations III, vol 36, Princeton University Press, pp 17–30

Paul C, Sommer U, Garzke J, et al (2016) Effects of increased CO2 concentration on nutrient limited coastal summer plankton depend on temperature. Limnol Oceanogr 61(3):853–868

Peace A, Zhao YQ, Loladze I, et al (2013) A stoichiometric producer-grazer model incorporating the effects of excess food-nutrient content on consumer dynamics. Math Biosci 244(2):107–115

Peace A, Wang H, Kuang Y (2014) Dynamics of a producer–grazer model incorporating the effects of excess food nutrient content on grazers growth. B Math Bbiol 76:2175–2197

Polis GA, Holt RD (1992) Intraguild predation: the dynamics of complex trophic interactions. Trends Ecol Evol 7(5):151–154

Prater C, Wagner ND, Frost PC (2017) Interactive effects of genotype and food quality on consumer growth rate and elemental content. Ecology 98(5):1399–1408

Pringle RM, Kartzinel TR, Palmer TM, et al (2019) Predator-induced collapse of niche structure and species coexistence. Nature 570(7759):58–64

Shu HY, Hu X, Wang L, et al (2015) Delay induced stability switch, multitype bistability and chaos in an intraguild predation model. J Math Biol 71:1269–1298

Sterner RW, Elser JJ (2017) Ecological stoichiometry: the biology of elements from molecules to the biosphere. In: Ecological stoichiometry. Princeton university press, New Jersey

Teurlincx S, Velthuis M, Seroka D, et al (2017) Species sorting and stoichiometric plasticity control community c: P ratio of first-order aquatic consumers. Ecol Lett 20(6):751–760

Thieme HR (1992) Convergence results and a poincaré-bendixson trichotomy for asymptotically autonomous differential equations. J Math Biol 30(7):755–763

Tong YD, Wang MZ, Peñuelas J, et al (2020) Improvement in municipal wastewater treatment alters lake nitrogen to phosphorus ratios in populated regions. P Natl Acad Sci USA 117(21):11566–11572

Wang H, Smith HL, Kuang Y, et al (2007) Dynamics of stoichiometric bacteria-algae interactions in the epilimnion. SIAM J Appl Math 68(2):503–522

841 Wang H, Sterner RW, Elser JJ (2012) On the “strict homeostasis” assumption in
842 ecological stoichiometry. Ecol Model 243:81–88

843 Wang H, Lu ZX, Raghavan A (2018) Weak dynamical threshold for the strict
844 homeostasis assumption in ecological stoichiometry. Ecol Model 384:233–240

845 Xie T, Yang XS, Li X, et al (2018) Complete global and bifurcation analysis of a
846 stoichiometric predatorprey model. J Dyn Differ Equ 30(2):1–26

847 Yan YW, Zhang JM, Wang H (2022) Dynamics of stoichiometric autotroph–
848 mixotroph–bacteria interactions in the epilimnion. B Math Biol 84(1):1–30

849 Yuan SL, Wu DM, Lan GJ, et al (2020) Noise-induced transitions in a nonsmooth
850 producer–grazer model with stoichiometric constraints. B Math Biol 82:1–22

851 Zhao XQ (2003) Dynamical systems in population biology, vol 16, Springer, New York